Dynamics of noise-induced wave-number selection in the stabilized Kuramoto-Sivashinsky equation

S. Saxena and J. M. Kosterlitz
Department of Physics, Brown University, Providence, Rhode Island 02912, USA

We revisit the question of wave-number selection in pattern-forming systems by studying the one-dimensional stabilized Kuramoto-Sivashinsky equation with additive noise. In earlier work, we found that a particular periodic state is more probable than all others at very long times, establishing the critical role of noise in the selection process. However, the detailed mechanism by which the noise picked out the selected wave number was not understood. Here, we address this issue by analyzing the noise-averaged time evolution of each unstable mode from the spatially homogeneous state, with and without noise. We find drastic differences between the *nonlinear* dynamics in the two cases. In particular, we find that noise opposes the growth of Eckhaus modes close to the critical wave number and boosts the growth of Eckhaus modes with wave numbers smaller than the critical wave number. We then hypothesize that the main factor responsible for this behavior is the excitation of long-wavelength ($q \to 0$) modes by the noise. This hypothesis is confirmed by extensive numerical simulations. We also examine the significance of the magnitude of the noise.

I. INTRODUCTION

Spatiotemporal patterns are ubiquitous in nature. Mathematically, they are represented by nonlinear partial differential equations that undergo a bifurcation from a spatially uniform steady state to periodic steady states with a continuous set of allowed wave numbers [1]. The band of allowed wave numbers is determined from a linear stability analysis of the equation of motion, and the wave number of the perturbation that grows fastest in the linear regime is called the critical wave number. The periodic steady states may themselves undergo secondary instabilities such as the Eckhaus instability [2], which occurs when the periodic states are subjected to long-wavelength perturbations. The states that are stable to such perturbations are said to be Eckhaus stable. Some well-known examples of pattern formation are Rayleigh-Bénard convection, Taylor-Couette flow, and cellular interfaces in directional solidification and eutectic growth [1,3–5]. Examples can also be found in chemistry (reaction-diffusion systems) and biology (chemotaxis-induced patterns in bacterial colonies) [1].

The existence of many apparently equivalent periodic states naturally leads to the question of wave-number selection. The two main aspects of the problem are as follows: (i) What is the wave number of an observed pattern for a specific set of experimental conditions? (ii) Is there a unique preferred wave number that is an intrinsic property of the system and does not depend on the initial state of the system? Most previous work on the subject has focused on deterministic mechanisms such as spatially ramped control parameters [6–8]. While control parameter ramps can be used to precisely tune the periodicity of the observed pattern, changing the ramping protocol leads to a *different* observed wave number [7,8]. In other words, the wave number selected by a control

parameter ramp is not unique. In a different direction, Schober *et al.* [9] have studied selection in the deterministic Swift-Hohenberg (SH) equation [10] by sampling over an ensemble of random initial conditions with the Fourier transform peaked about a specific wave number $\bar{q}$. Again, the final state was found to depend on the value of $\bar{q}$. These results have been used to argue that there is no universal selection mechanism.

On the other hand, *stochastic* wave-number selection, i.e., selection in the presence of noise, has historically been a topic of debate. One of the first studies of stochastic selection was performed by Kerszberg [11,12]. The author studied the evolution of a periodic cellular interface in a model of directional solidification with additive noise and found that the noise induces creation or destruction of cells, driving the interface toward a unique periodicity. Some qualitative arguments to explain this effect were given. More detailed studies have been performed recently in a model known as the stabilized Kuramoto-Sivashinsky (SKS) equation [13–15]. In Ref. [13], the authors used the least action principle to calculate the probability of transitions between the different steady states. In Ref. [15], the stationary probability of being in a particular periodic state at long times was calculated. The probability was found to be greatest for a particular periodic state. This state was independent of the initial conditions and the noise strength, as long as the noise was large enough to allow the system to explore all the available states. This is in stark contrast to the deterministic mechanisms mentioned above.

Selection of a unique wave number by noise is expected for dynamics where the deterministic part is the gradient of a free energy functional: $\partial_t u(x, t) = -\delta \mathcal{F}[u]/\delta u(x, t) + \zeta(x, t)$. In that case, it is known that the most probable configuration is the one that minimizes the free energy. The primary example of this is the SH model [10], for which the free energy is minimized by a periodic configuration with wave number

$q_{\min}$, which is very close to the critical wave number of that model [16]. In the presence of noise, the wave number of the most probable configuration is found to be very close to $q_{\min}$ [17], although it is impossible to distinguish between $q_{\min}$ and the critical wave number for the simulation parameters used in these studies.

The SKS equation, on the other hand, does *not* possess a free energy functional, and a clear understanding of what makes one steady state preferable compared to others is lacking. Although we have established that there is a unique, preferred wave number for the SKS problem [15], and identified it for various parameters, a detailed investigation of the dynamical processes leading to the selection has not been performed, to our knowledge. This is the goal of this work. We shift our focus from the stationary probability distributions of Ref. [15] to the time evolution of the various Fourier components of the solution of the SKS equation. By doing so, we identify the key process responsible for noise-induced selection in the SKS model. Through a detailed numerical analysis, we show that the noise fundamentally alters the nonlinear dynamics of the SKS equation in two ways. First, it causes the growth of modes with wave numbers close to zero in the nonlinear regime. Second, it couples these small wave-number modes with the Eckhaus stable modes in a way that opposes the growth of modes close to the critical one. These effects do not occur without noise and highlight the importance of noise in constraining the periodicity of patterns.

The rest of the paper is organized as follows: In Sec. II, we introduce the deterministic and stochastic SKS equations in one dimension, and we review the results of Ref. [15]. In Sec. III, we study how the amplitudes of the Fourier components of the solution evolve *in time*, and we identify important differences between the deterministic and stochastic cases. We also compare the new results with those of Ref. [15], and we examine the role of the strength of the noise. In Sec. IV, we provide a qualitative explanation for the findings of Sec. III followed by a detailed quantitative analysis. Finally, in Sec. V, we summarize our results and mention potential directions for future work.

II. BACKGROUND

A. Deterministic dynamics

We review here the dynamics of the deterministic SKS equation. In one dimension, it reads

$$\partial_t u(x,t) = F[u] = \left(-\alpha - \partial_x^2 - \partial_x^4 \right) u + (\partial_x u)^2. \quad (1)$$

Here, α is the control parameter and $u(x,t)$ is a dimensionless field of dimensionless space-time variables. This equation arises in various situations, such as directional solidification and the Burton-Cabrera-Frank model of terrace edge growth [18,19]. Applying a periodic perturbation with wave number q and linearizing Eq. (1) yields the linear dispersion relation for the growth rate $\sigma(q) = -\alpha + q^2 - q^4$. The growth rate is positive for a range of wave numbers whenever $\alpha \leqslant 1/4$. The wave number that maximizes $\sigma(q)$ is the critical wave number $q_c = 1/\sqrt{2}$. As an example, the linear dispersion relation is shown in Fig. 1 for $\alpha = 0.20$. In this case, $\sigma(q)$ is positive for $0.53 \leqslant q \leqslant 0.85$. We also show the Eckhaus stable wave numbers in Fig. 1, which satisfy $q_E^- \leqslant q \leqslant q_E^+$.
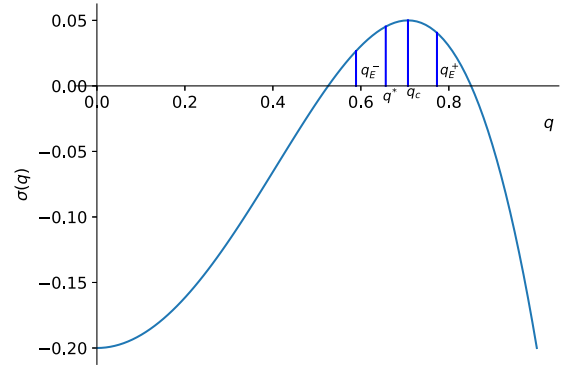

FIG. 1. Sketch showing the linear growth rate of periodic perturbations $\sigma(q)$ as a function of wave number q for the stabilized Kuramoto-Sivashinsky equation, with $\alpha = 0.20$. The critical wave number is $q_c = 1/\sqrt{2}$ and the noise-selected wave is $q^\star$. The boundaries of the Eckhaus band are at q_E^- and q_E^+.

A typical deterministic steady state with wave number q consists of a fundamental mode, and small terms containing the second and higher harmonics. It can be written in the following form [18]:

$$u_{q,\det}(x) = \sum_{l=-\infty}^{\infty} \widetilde{u}_{lq} e^{ilqx}, \quad (2)$$

where the subscript "det" stands for "deterministic." We show the position space and Fourier space representations of a state with wave number $q = \bar{q} = 0.6627$ in Figs. 2(a) and 2(b). In position space, the pattern looks sinusoidal and oscillates about a nonzero value. In Fourier space, there is a large peak at $q = \bar{q}$, a smaller one at $q = 2\bar{q}$, and a very small one at $q = 3\bar{q}$. There is also a peak at $q = 0$ because of the nonzero spatial average of $u(x,t)$. The presence of this peak has no effect on our results. Henceforth, when we refer to a state with wave number q, we mean that the Fourier transform of the state has the largest peak at wave number q.

B. Previous results on selection in the stochastic SKS equation

The stochastic SKS equation reads

$$\partial_t u(x,t) = F[u] + \zeta(x,t), \quad (3)$$

where $\zeta(x,t)$ is Gaussian uncorrelated noise satisfying $\langle \zeta(x,t) \rangle = 0$ and $\langle \zeta(x,t)\zeta(x',t') \rangle = 2\varepsilon\delta(x-x')\delta(t-t')$. In Ref. [15], Eq. (3) was integrated using a Fourier-spectral method on a lattice consisting of N points, separated by a distance h [20,21]. The system size is $L = Nh$. Equations of evolution for the discrete Fourier transform (DFT) of the field $u(x,t)$ were obtained from Eq. (3). The DFT is defined as

$$\widetilde{u}_n(t) = \sum_{m=0}^{N-1} u_m(t) \exp\left[\frac{-2\pi i m n}{N} \right];$$
$$n = 0, 1, \ldots, N/2 - 1, -N/2, \ldots, -1, \quad (4)$$

where u_m is the discretized field in position space, i.e., $u_m = u(x = x_m = mh)$. Each n corresponds to a wave number q_n
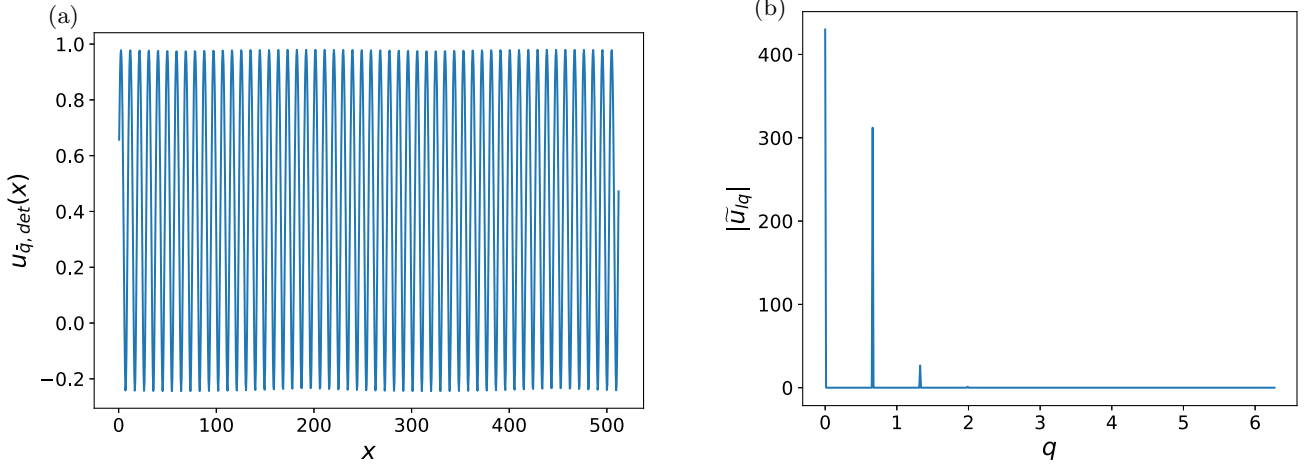
FIG. 2. (a) Steady-state configuration $u_{\bar{q},\mathrm{det}}(x)$ for $q = \bar{q} = 0.6627$. (b) The discrete Fourier transform of $u_{\bar{q},\mathrm{det}}(x)$, with peaks at $\bar{q}$, $2\bar{q}$, and $3\bar{q}$. Higher harmonics are present but too small to be seen.

given by

$$q_n = \frac{2\pi n}{L} = n\Delta q. \tag{5}$$

Because of the discreteness of the allowed wave numbers, our estimate of the selected wave number contains an uncertainty equal to the quantity Δq [15]. This uncertainty can be reduced by increasing the system size L, as can be seen from Eq. (5).

The equation of motion for the nth Fourier component $\widetilde{u}_n$ can be shown to be [15,20,21] (see also Appendix B)

$$\frac{d\widetilde{u}_n}{dt} = -\alpha\widetilde{u}_n + (2\pi n/L)^2\widetilde{u}_n - (2\pi n/L)^4\widetilde{u}_n \\ + \widetilde{\mathbf{N}}_n + \widetilde{\zeta}_n, \tag{6}$$

where $\widetilde{\mathbf{N}}_n$ is the nth component of the DFT of the nonlinear term $(\partial_x u)^2$ defined by

$$\widetilde{\mathbf{N}}_n = \sum_{m=0}^{N-1}(\partial_x u)_m^2 e^{-2\pi imn/N} \tag{7}$$

and $(\partial_x u)_m^2$ is the value of the square of the spatial derivative of u at $x = x_m = mh$. Let $v(x)$ denote the function $\partial_x u(x)$. The nth component of the DFT of $v(x)$ can be shown to be (Appendix B)

$$\widetilde{v}_n = 2\pi in\widetilde{u}_n/L; \quad -N/2 + 1 < n < N/2 - 1, \tag{8}$$

where $\widetilde{v}_0$ and $\widetilde{v}_{N/2}$ are zero and we have assumed that N is even.

Using the discrete convolution theorem, it can be shown that the DFT of the term $(\partial_x u)^2$ is (Appendix B)

$$\widetilde{\mathbf{N}}_n = \left(\frac{1}{N}\right)\left(\frac{2\pi}{L}\right)^2 \sum_{n_1=-N/2+1}^{N/2-1} \widetilde{v}_{n_1}\widetilde{v}_{n-n_1}. \tag{9}$$

The system of Eqs. (6) was solved over very long times using a semi-implicit integration scheme [22] with time step $\Delta t = 0.3$. To find the selected wave number, we counted the number of times a periodic state of wave number q_n was visited over a *single long trajectory* and plotted a histogram of all the states visited. Dividing the number of hits in each state

by the total time of integration gave the fraction of time spent in each state, which approaches the stationary probability distribution of states if the run time is very long.

To do so, it was necessary to define the state of the system in the presence of noise. A typical configuration $u(x)$ and the corresponding power spectrum $|\widetilde{u}_n|$ are shown in Figs. 3(a) and 3(b). The noise broadens the peaks in the power spectrum, but one can still discern the fundamental harmonic and second-harmonic peaks. In position space the field is irregular, but it retains its cellular nature. Based on these observations, we adopted the following criterion: the system was considered to be in a state with wave number $q_n = 2\pi n/L$ at time t if

$$|\widetilde{u}_n(t)| \geqslant 2|\widetilde{u}_{n'}(t)| \text{ for all } n' \neq n, \tag{10}$$

where both n and n' are nonzero. This criterion ensured that only those states were counted in which one mode was much larger than all others, and highly disordered configurations with several wave numbers having roughly the same Fourier amplitude were disregarded.

With this standard for determining the instantaneous state of the system, Eqs. (6) were integrated for $0.16 < \alpha < \alpha_c$. This range of α was chosen because many complicated configurations, such as parity breaking states and breathing modes, are possible when α is less than 0.16 [18] (see Appendix B). Taking our computational resources into account, the run time was fixed at $T \approx 2 \times 10^8 \Delta t = 5 \times 10^7$ for all the simulations. To obtain accurate stationary probability distributions of wave numbers, we defined a threshold noise strength $\varepsilon_{\min}(\alpha, N, T)$ above which the entire set of states could be sampled and stationary histograms could be attained. The arguments emphasize that $\varepsilon_{\min}$ depends not only on α but also on the run time and the system size. It is thus a practical choice that is dictated by computational restraints. For example, increasing the run time T while keeping α and N fixed leads to a smaller value of $\varepsilon_{\min}$. On the other hand, increasing N while keeping T fixed increases $\varepsilon_{\min}$. By fixing the system size N and simulation time T, we determined $\varepsilon_{\min}$ for each α. Setting $\varepsilon \geqslant \varepsilon_{\min}$ in Eqs. (6), stationary histograms were obtained and the wave number with the maximum number of hits was designated as the *selected wave number*, $q^\star$. As long as the noise strength was above the threshold value, $q^\star$ was
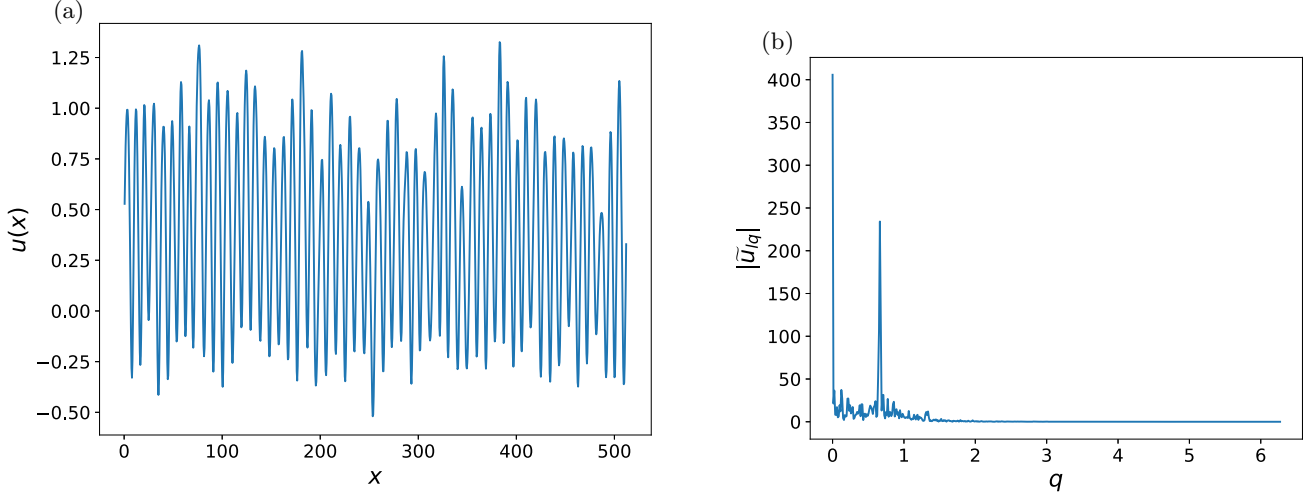
FIG. 3. (a) Typical field configuration $u(x, t)$ for $\alpha = 0.20$ and $\varepsilon = 0.004$. (b) Typical configuration in Fourier space as a function of the integer n. The corresponding wave number is given by $q_n = 2\pi n/L$.

found to be independent of initial conditions and the noise strength.

A variety of initial conditions were tested, for example by placing the system initially in the q_c state, the $q^\star$ state, or a superposition of sinusoids with different wave numbers. We also used some other criteria to define the instantaneous state, such as the number of extrema (crests and troughs) in the pattern. The histograms using this criterion yielded the same selected wave number. Thus, $q^\star$ was identified as a characteristic property of the SKS equation. *For brevity, we will refer to the methodology of Ref. [15] as the "histogram method."*

We tabulate the values of $q^\star$ in Table I for convenience.

III. ANALYSIS OF DYNAMICS

The histograms of Ref. [15] were obtained by integrating Eq. (3) once and computing the fraction of time spent in each state. While this yields a stationary probability distribution of wave numbers, it does not give any information about how the stationary distribution is reached and why the selected wave number is different from the critical one. It is clear that a careful analysis of the *time evolution* of Eq. (3) is necessary to understand how selection occurs.

For this purpose, it is natural to focus on the time evolution of the structure function $S_n(t) = \langle|\widetilde{u}_n(t)|^2\rangle = \langle\widetilde{u}_n(t)\widetilde{u}_{-n}(t)\rangle$, where the angular brackets denote an average over independent trajectories. Using Eq. (3), we can derive an equation for

TABLE I. Noise-selected wave numbers as found in Ref. [15].

Control parameter α	$q^\star$ ($L = 2000$)
0.24	0.6974 ($n^\star = 222$)
0.22	0.6754 ($n^\star = 215$)
0.20	0.6566 ($n^\star = 209$)
0.17	0.6377 ($n^\star = 203$)

the time derivative of S_n as follows:

$$\dot{S}_n(t) = \langle\dot{\widetilde{u}}_n(t)\widetilde{u}_{-n}(t)\rangle + \langle\widetilde{u}_n(t)\dot{\widetilde{u}}_{-n}(t)\rangle. \tag{11}$$

The dot denotes the time derivative. Using Eqs. (6) and (9), we obtain

$$\dot{S}_n(t) = 2\sigma_n S_n(t) + \langle\widetilde{u}_n\widetilde{\zeta}_{-n}\rangle + \langle\widetilde{u}_{-n}\widetilde{\zeta}_n\rangle$$
$$+ \frac{1}{N}\left[\sum_{n_1=-N/2+1}^{N/2-1}\langle\widetilde{v}_{n_1}\widetilde{v}_{-n-n_1}\widetilde{u}_n\rangle\right.$$
$$\left.+ \sum_{n_1=-N/2+1}^{N/2-1}\langle\widetilde{v}_{n_1}\widetilde{v}_{n-n_1}\widetilde{u}_{-n}\rangle\right], \tag{12}$$

where $\sigma_n = -\alpha + q_n^2 - q_n^4$ is the linear operator appearing in Eq. (3). We can split the sums over n_1 as follows:

$$\sum_{-N/2+1}^{N/2-1} = \sum_{-N/2+1}^{-1} + \sum_{1}^{N/2-1}. \tag{13}$$

The term in square brackets in Eq. (12) then becomes

$$\sum_{n_1=-N/2+1}^{-1}\langle\widetilde{v}_{n_1}\widetilde{v}_{-n-n_1}\widetilde{u}_n\rangle + \sum_{n_1=1}^{N/2-1}\langle\widetilde{v}_{n_1}\widetilde{v}_{-n-n_1}\widetilde{u}_n\rangle$$
$$+ \sum_{n_1=-N/2+1}^{-1}\langle\widetilde{v}_{n_1}\widetilde{v}_{n-n_1}\widetilde{u}_{-n}\rangle + \sum_{n_1=1}^{N/2-1}\langle\widetilde{v}_{n_1}\widetilde{v}_{n-n_1}\widetilde{u}_{-n}\rangle. \tag{14}$$

The second and third terms of Eq. (14) are complex conjugates, as are the first and last terms. Since $z + z^\star = 2\operatorname{Re}(z)$ for a given complex number z, the above reduces to

$$\sum_{n_1=1}^{N/2-1} 2\operatorname{Re}\langle\widetilde{v}_{n_1}\widetilde{v}_{-n-n_1}\widetilde{u}_n\rangle + (n \to -n).$$

TABLE II. List of important symbols and their meanings.

Symbol	Meaning
T	Time over which the number of hits in each state was measured in Ref. [15]
$\varepsilon_{\min}(\alpha, N, T)$	Minimum noise needed to explore all states and obtain stationary histograms in one trajectory of length T, for fixed α and N
$q^\star = 2\pi n^\star / L$	Selected wave number when ($\varepsilon \geqslant \varepsilon_{\min}$) found in Ref. [15]
T_{S0}	Duration of each trajectory in the ensemble of trajectories over which S_n is calculated when $\varepsilon = 0$. Fixed at $1.2 \times 10^5 = 4 \times 10^5 \Delta t$
T_S	Duration of each trajectory in the ensemble of trajectories over which S_n is calculated for $\varepsilon \neq 0$. Fixed at $1.2 \times 10^6 = 4 \times 10^6 \Delta t$
$q_{S0} = 2\pi n_{S0}/L$	Most probable wave number identified as the maximum of the structure function S_n at time T_{S0} for the noiseless case
$q_S(\alpha, \varepsilon, T_S) = 2\pi n_S(\alpha, \varepsilon, T_S)/L$	Most probable wave number identified as the maximum of the structure function S_n at time T_S for given noise strength ε

Substituting this expression into Eq. (12), we get the expression for the time derivative of the structure function,

$$\dot{S}_n(t) = 2\sigma_n S_n(t) + 2 \operatorname{Re} \langle \widetilde{u}_n \widetilde{\zeta}_{-n} \rangle$$
$$+ \sum_{n_1=1}^{N/2-1} [2 \operatorname{Re} \langle \widetilde{v}_{n_1} \widetilde{v}_{-n-n_1} \widetilde{u}_n \rangle + (n \to -n)]. \quad (15)$$

We can make this expression more compact by defining

$$\mathcal{S}_{n,n_1} = 2 \operatorname{Re} \langle \widetilde{v}_{n_1} \widetilde{v}_{-n-n_1} \widetilde{u}_n \rangle \quad (16)$$

and

$$\mathcal{N}_n = \frac{1}{N} \sum_{n_1=1}^{N/2-1} (\mathcal{S}_{n,n_1} + \mathcal{S}_{-n,n_1}). \quad (17)$$

Equation (15) then reduces to

$$\dot{S}_n(t) = 2\sigma_n S_n(t) + 2 \operatorname{Re} \langle \widetilde{u}_n \widetilde{\zeta}_{-n} \rangle + \mathcal{N}_n. \quad (18)$$

Finally, we note that from Novikov's theorem [23], $\langle \widetilde{u}_n \widetilde{\zeta}_{-n} \rangle$ is simply a constant proportional to ε. Therefore, this term only contributes a constant to Eq. (18) and will henceforth be ignored.

From Eq. (18), it is clear that the linear dynamics of the structure function are identical to those of the deterministic SKS equation, with twice the linear growth rate. To understand the effects of the noise, we must therefore study the *nonlinear* dynamics of $S_n(t)$ for various values of n. We do this by integrating Eq. (3) for several independent noise realizations over a fixed time interval and averaging over all the realizations to yield the time evolution of the structure function. Note that it is also possible to integrate Eq. (18) directly, but one would require an appropriate truncation scheme to do so. We do not pursue this method here.

We study two cases of interest. First, we obtain $S_n(t)$ with random initial conditions and zero added noise, i.e., $\varepsilon = 0$. Then we repeat the same procedure, but with $\varepsilon \neq 0$. In each case, we identify a dominant wave number as the one that maximizes S_n at the end of the simulation, and we compare it with the results of the histogram method [15]. The difference in the dynamics of S_n for the two cases will shed light on the nature of the selection process. The simulations of the structure function are carried out over time intervals that are shorter than those of the histogram simulations, for reasons explained

below. These time scales and other important symbols are given in Table II.

A. Noiseless dynamics with random initial conditions

We set $\alpha = 0.20$, $\varepsilon = 0$, and use random initial conditions drawn from a Gaussian distribution. The lattice consists of $N = 4000$ points, separated by distance $h = 0.5$. We use the same semi-implicit time integration scheme as Ref. [15] with time step $\Delta t = 0.3$, and we integrate Eq. (3) from time $t = 0$ to time $t = T_{S0} = 1.2 \times 10^5$ for 180 independent runs. The subscript $S0$ signifies that we are calculating S_n with zero noise. This calculation is computationally demanding, forcing us to use a run time that is much shorter than that used in Ref. [15] (see Table II).

For our parameters, the Eckhaus band is given by $n_E^- \leqslant n \leqslant n_E^+$, with $n_E^- = 188$ and $n_E^+ = 246$. This corresponds to $0.589 \leqslant q \leqslant 0.767$. The critical wave number is $q_c = 2\pi n_c/L \approx 1/\sqrt{2}$, where $n_c = 225$, and the selected wave number determined from the histogram method is $q^\star = 2\pi \times n^\star/L = 0.6566$, where $n^\star = 209$ [15].

In Fig. 4(a), we show the structure function for $\alpha = 0.20$ and various values of n, including $n = n^\star$ and $n = n_c$. S_{221} and S_{222} are found to have the largest long-time values, with S_{222} being slightly larger. $S_{n^\star}$ and S_{210} decay to very small values, as does S_{n_c}. In Figs. 4(b) and 4(c), we take a closer look at the early and intermediate time dynamics. At very early times [Fig. 4(b)], S_{n_c} grows faster than all the others, followed by S_{220}, S_{221}, and S_{222}. The growth of $S_{n^\star}$ and S_{210} is much slower. This is consistent with the fact that the structure function has the same linear dynamics as the deterministic SKS equation. Around $t \approx 180$, we can see the growth of S_{220}, S_{221}, S_{222}, and S_{n_c} slowing down, marking the beginning of the nonlinear regime. A short time later, the growth of S_{n_c} becomes slower and slower [Fig. 4(c)]. S_{220}, S_{221}, and S_{222} overtake S_{n_c}, while $S_{n^\star}$ and S_{210} start decreasing. Qualitatively, this occurs because the nonlinear terms (which oppose growth) in the equation of motion for $S_{n^\star}$ and S_{210} exceed the linear terms (which favor the growth), rendering the time derivatives $dS_{n^\star}/dt$ and dS_{210}/dt negative. Thus, $S_{n^\star}$ and S_{210} decay to zero.

We conclude that starting from random initial conditions, the system is most likely to end up in a periodic state with wave number $2\pi \times 221/L$ or $2\pi \times 222/L$. In other words,
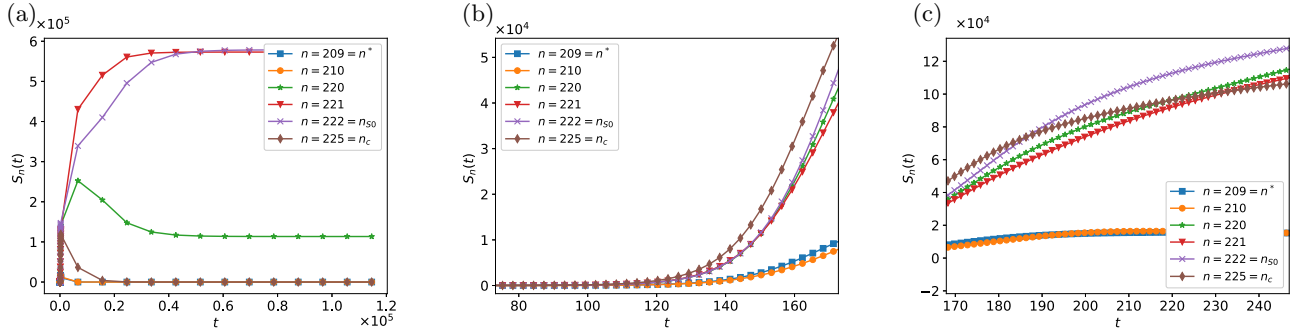
FIG. 4. (a) Time evolution of $S_n(t)$ with random initial conditions and $\varepsilon = 0$. (b) The early time regime. (c) Intermediate time regime.

these are the states that are most likely to be realized for typical initial conditions, if the evolution is purely deterministic. We use the symbol n_{S0} to refer to the $n = 222$ state, meaning that it is the wave number for which S_n is maximum when $\varepsilon = 0$.

On the other hand, the state with $n = n^\star$, which was the noise-selected state in Ref. [15], has a very small probability, as seen from the fact that $S_{n^\star}$ is negligible at the end of integration. The same is true for $n = 210$.

B. Stochastic dynamics

Next, we repeat the above procedure with $\varepsilon \neq 0$, using random initial conditions as in the previous subsection. For $\alpha = 0.20$, $\varepsilon_{\min}$ was found to be approximately equal to 0.003 [15]. Here, we set $\varepsilon_{\min} = 0.004$, which is slightly greater than $\varepsilon_{\min}$. To get a sense of how strong this noise is, we show a scatter plot of the wave number with the maximum power at each time for *a single run*. The system initially undergoes transitions between several disordered states at different Eckhaus stable wave numbers. The states at the edges of the Eckhaus band are very unstable. After about 10^5 time steps, the system enters a dynamical regime in which only a few states are visited. This is illustrated in Fig. 5(a) over the time interval $70\,000 \leqslant t \leqslant 205\,000$. There are rapid transitions among the $n = 209$, 210, and 211 states, along with rare transitions to $n = 212$. After $t \approx 150\,000$, the $n = 211$ state is visited less frequently, and frequent transitions to $n = 208$ occur. We show an enlarged view of the window between $t = 168\,000$ and $182\,000$ in Fig. 5(b). We also show a spatiotemporal

portrait of $u(x)$ in Fig. 5(c), although the transitions are hard to see in position space.

We now compute $S_n(t)$ by averaging over 180 integrations of Eq. (3). This time, the integration runs from $t = 0$ to $t = T_S = 1.2 \times 10^6$. This is an order of magnitude larger than T_{S0} because the time taken for one dominant mode to emerge from several competing ones is larger when the noise is nonzero, as we will see in Fig. 6. We want to determine the state with the maximum value of the structure function at time T_S, denoted by n_S. The results are shown in Fig. 6(a). We now see that $S_{n^\star}$ and S_{210} attain the largest long-time values, while S_{220}, S_{221}, and $S_{n_{S0}}$ decay to small (but nonzero) values. S_{n_c} is always very small.

Figure 6(b) shows the evolution of $S_n(t)$ at early times. S_{220} and S_{210} are seen to grow fastest even in this early time regime, followed by S_{n_c}. Clearly, our chosen ε is so large that the linear regime is obscured in our simulation. After $t \approx 80$ [Fig. 6(c)], the growth of S_{220}, S_{221}, $S_{n_{S0}}$, and S_{n_c} slows down, while $S_{n^\star}$ and S_{210} keep growing. This suggests that the nonlinear terms in Eq. (18) for $n = 220$, 221, 222 (n_{S0}) and $n = n_c$ surpass the linear terms in the presence of the noise. These modes decrease at intermediate times before attaining a small steady-state value at $t = T_S$. For wave numbers near $n^\star$, the nonlinear term does not exceed the linear term, and the structure function simply saturates at a large value at long times. The $n = 209$ state is the one that maximizes S_n, and hence $n_S = 209$. For this noise strength, n_S is identical to $n^\star$.

To summarize, for an ensemble of noiseless trajectories starting from random configurations, the most probable wave number n_{S0} is very close to n_c. The corresponding
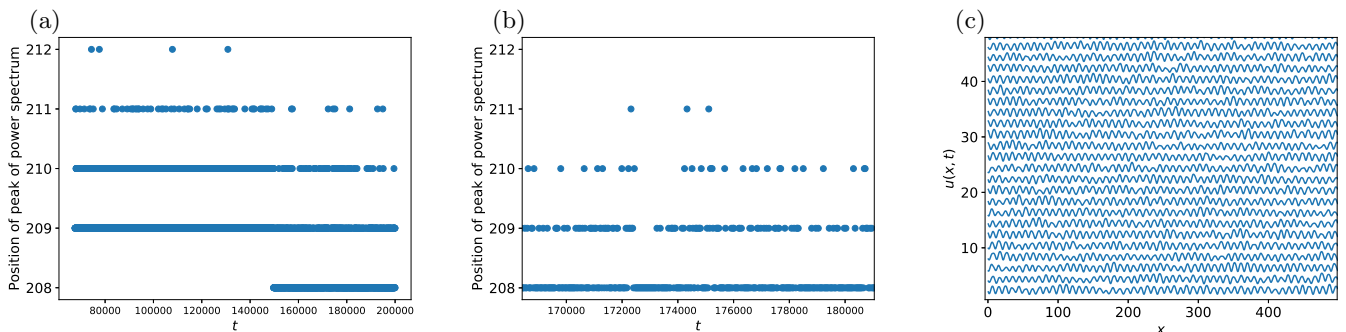

FIG. 5. (a) Maximum of power spectrum as a function of time, with $\alpha = 0.20$ and $\varepsilon = 0.004$. (b) Magnified view of the time interval $168\,000 \leqslant t \leqslant 181\,000$. (c) Temporal evolution of $u(x, t)$ for $0 \leqslant x \leqslant 500$ over the time interval $168\,000 \leqslant t \leqslant 181\,000$.
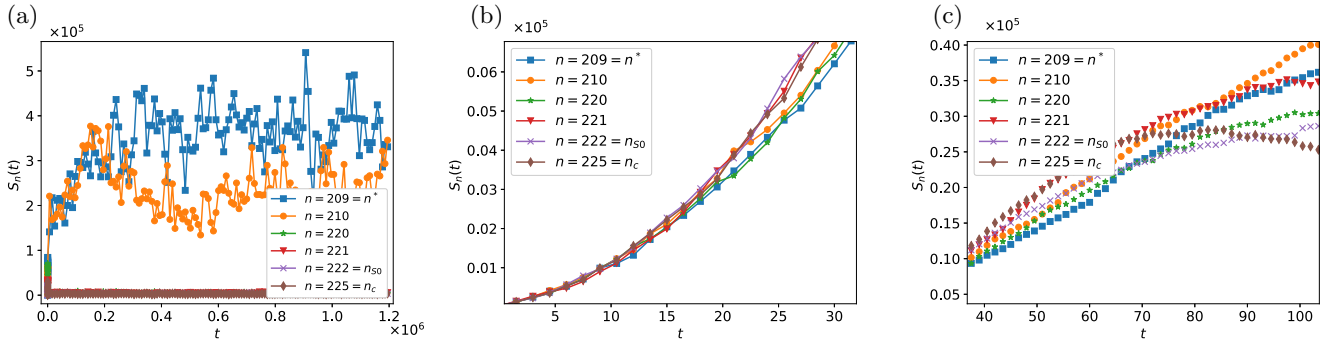
FIG. 6. (a) S_n as a function of time t when $\varepsilon = 0.004$. (b) Early time dynamics. (c) Intermediate time dynamics.

component of the structure function grows rapidly in the nonlinear regime, while the component corresponding to $n^\star$ decays in the nonlinear regime. However, when $\varepsilon \geqslant \varepsilon_{\min}$, the situation is reversed and $S_{n^\star}$ grows nonlinearly, while $S_{n_{S0}}$ decays. This is consistent with the findings of Ref. [15], which were obtained from *long-time* averaging of the number of hits in each state. Before attempting to explain this reversal of dynamics, however, we investigate how the structure function dynamics are changed by the magnitude of ε.

C. Effect of varying the noise strength

We vary the noise strength over several orders of magnitude and determine n_S at time $T_S = 1.2 \times 10^6$, as shown in Fig. 7. We study the following two cases separately: (i) strong noise, i.e., $\varepsilon \geqslant \varepsilon_{\min}$; and (ii) weak noise, $\varepsilon < \varepsilon_{\min}$. Recall that $\varepsilon_{\min}$ was determined in Ref. [15] for one run of duration T.

1. High noise strength

This case is represented by the last three points in Fig. 7. As long as $\varepsilon \geqslant \varepsilon_{\min}$, the most probable wave number obtained from the structure function approach, i.e., n_S, *is the same as selected wave number $n^\star$ obtained from the histogram method [15]*. It is independent of noise strength and initial conditions. In a sense, for all $\varepsilon \geqslant \varepsilon_{\min}$, there is an intrinsic wave number

unique to the SKS equation, which can be obtained by time averaging [15] as well as trajectory averaging.

2. Low noise strength

Below $\varepsilon_{\min}$, n_S increases slowly to values above $n^\star$, as ε is decreased. However, the evolution of $S_n(t)$ is slow in this case and does not reach a steady state in time T_S. To see this, we perform a simulation for ε slightly less than $\varepsilon_{\min}$ using the histogram method of Ref. [15]. We choose $\varepsilon = 0.0027$ for which the structure function approach gives a most probable wave number $n_S = 211$; cf. Fig. 7. The histograms at various times are shown in Fig. 8. After some initial transients, the system enters the $n = 213$ state, and then transitions to the $n = 212$ state at time $t = 4000$, where it remains stuck for a long time. At $t = 1.6 \times 10^7$ (stars in Fig. 8), the system makes frequent jumps to the $n = 210$ and 211 states, but the peak of the histogram stays at $n = 212$. By $t = 3.9 \times 10^7$, the system is in the $n = 210$ state for most of the time, and a prominent peak appears at this wave number (pluses in Fig. 8). Just before the end of the integration at $t = T$, the histogram has a peak at $n = n^\star = 209$, but it is still changing with time. It is then reasonable to conclude that the histogram is approaching a stationary form peaked about $n = n^\star$ for $\varepsilon = 0.0027$. Since the structure function approach gives a dominant wave number of $n_S = 211 > n^\star$ for the same ε at $t = T_S$, we infer that it has not yet reached a stationary state at $t = T_S$. Thus, *we can no longer find a unique "selected wave number" that is*
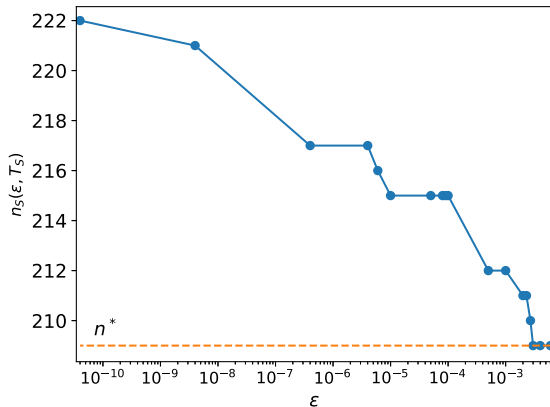

FIG. 7. $n_S(\varepsilon, T_S)$ obtained from the time evolution of S_n for different ε. For $\varepsilon \geqslant \varepsilon_{\min}$, n_S is a constant, equal to $n^\star$. For $\varepsilon < \varepsilon_{\min}$, a stationary state cannot be reached in time T_S. In this case, n_S depends on ε and T_S.
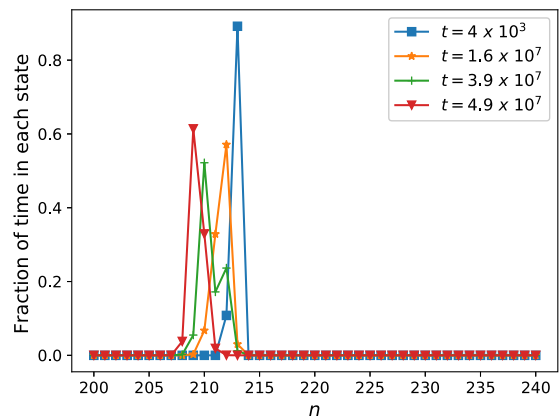

FIG. 8. Histograms at various times during one long run from $t = 0$ to $t = T$, with $T = 5 \times 10^7$. Here $\varepsilon = 0.0027 < \varepsilon_{\min}$.
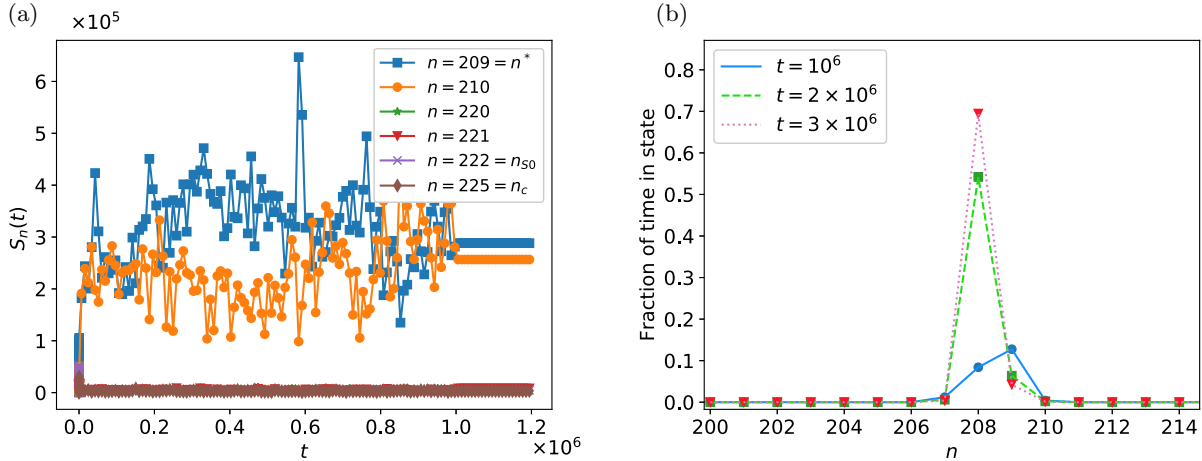
FIG. 9. (a) $S_n(t)$ when the noise is turned off at $t = 10^6$. (b) Typical histograms at various times for a single run.

identical for time averages and trajectory averages. Instead, the structure function approach yields the "most probable" or "dominant" wave number $q_S(\varepsilon, T_S)$, which need not be equal to $q^\star$. The arguments in parentheses emphasize that q_S is a function of ε and T_S when $\varepsilon < \varepsilon_{\min}$, and it does not represent a characteristic property of the SKS equation. As we decrease ε further, it becomes harder to reach a steady state with either the histogram method or the structure function method. In particular, the results of the histogram method become strongly dependent on initial conditions.

D. Turning off the noise at intermediate times

We have also investigated what happens if the noise is turned off at some late time. We obtain the time evolution of S_n for $\alpha = 0.20$ with $\varepsilon = 0.004$, but set ε to zero at $t = 10^6$. In Fig. 9(a), we can see that after the noise is turned off, the system settles into one of the deterministic steady states with $n = 208, n^\star$ or 210. The $n = n^\star$ state continues to be more probable than $n = 208$ and 210.

On the other hand, if we use the histogram method, turning off the noise at some time will make the system settle in the deterministic state that is closest to its configuration at the instant the noise was turned off. We show this for a typical trajectory [Fig. 9(b)]. At $t = 10^6$, when the noise is just turned off, the maximum of the histogram is at $n = n^\star$. However, the configuration at that particular instant is closest to the $n = 208$ state. Hence, as soon as the noise is turned off, the system collapses into the $n = 208$ state. Following this, the histogram develops a peak at $n = 208$ that gets progressively sharper with time. If we were to repeat this simulation again, the system could settle into a different state, depending on the configuration when the noise is turned off.

In summary, we have seen that the noise alters the non-linear behavior of our model in a nontrivial manner. Its main effect is to make configurations with wave number less than q_c more probable. For $\varepsilon \geqslant \varepsilon_{\min}$, there is a selected wave number that is an intrinsic property of the SKS equation. For $\varepsilon < \varepsilon_{\min}$, neither a stationary histogram nor a stationary structure function can be obtained, and one can only find a most probable wave number for a given noise amplitude, time, and averaging procedure.

Irrespective of whether ε is greater than or less than $\varepsilon_{\min}$, the dominant wave number in Fig. 7 is always less than the critical wave number. In the following sections, we will focus on understanding why this is the case.

IV. MECHANISM OF WAVE-NUMBER SELECTION

To understand how the noise shifts the dominant wave number to values less than q_c, it is useful to plot $\sqrt{S_n}$ versus n at $t = T_S$, as shown in Fig. 10. $\sqrt{S_n}$ is large for $n_E^- \leqslant n \leqslant n_E^+$ as well as for n values lying slightly outside this interval. However, the inset of Fig. 10 shows that it is large even for $n \leqslant 100$, which is far outside the Eckhaus stable band. Moreover, it *increases* as n decreases, becoming comparable to the second-harmonic peak. The modes with $n < n_E^-$ quickly decay to zero in purely deterministic evolution (with the exception of $n = 0$, which we disregard) and cannot grow without noise. We hypothesize that this effect is responsible for the observations of the previous section.

To test this hypothesis, we remove the effect of the small wave numbers by repeating the stochastic simulations, but this time setting the modes with n lying between 1 and 50 to zero at each time step. This is equivalent to suppressing wave numbers between 0.003 and 0.157. We retain the $n = 0$ mode because it is a feature of the deterministic problem. We
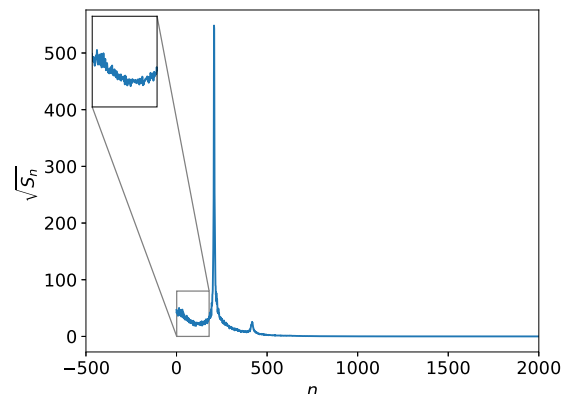

FIG. 10. Long-time noise-averaged power spectrum for $\alpha = 0.20$ and $\varepsilon = 0.004$. Inset: amplification of modes near $n = 0$.
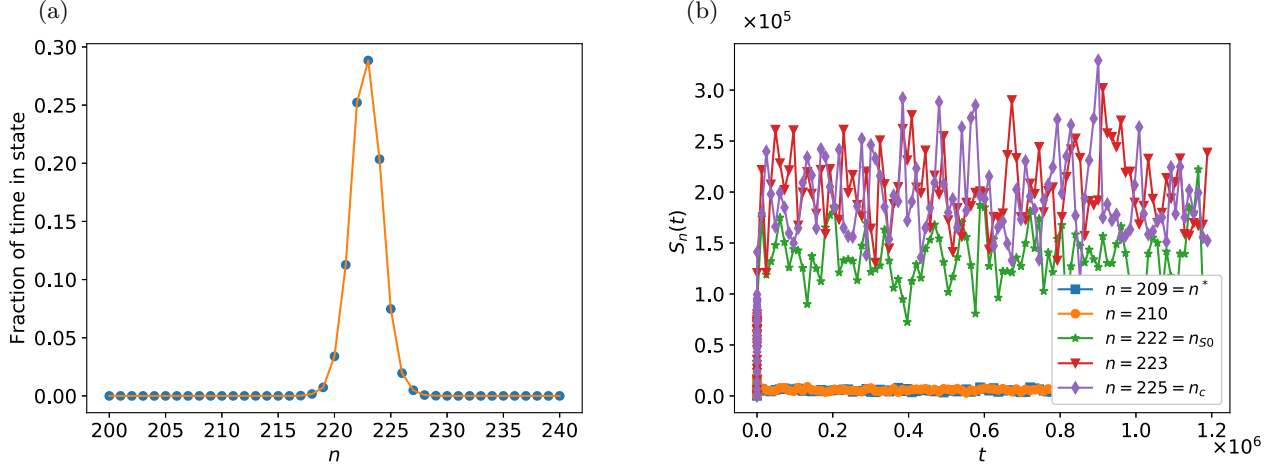
FIG. 11. (a) Stationary probability distribution of wave numbers for $\alpha = 0.20$ and $\varepsilon = 0.004$ obtained from one long trajectory, but with modes between $n = 1$ and 50 ignored. The new selected wave number corresponds to $n = 223$ as opposed to $n = 209$ in the original dynamics. (b) Time evolution of S_n. The state with $n = 209$, which was selected in the unmodified dynamics, is now highly improbable at long times. The most dominant modes are $n = 222$, 223, and 224. This is clearly evident in spite of the noisiness.

obtain the selected wave number from the histogram method of Ref. [15] and the time evolution of $S_n(t)$ as in Sec. III.

We see immediately that the histogram for the "modified" dynamics is peaked about a *different* selected wave number $q^{\star\prime}$, which is very close to q_c [Fig. 11(a)]. On the other hand, the structure function dynamics in Fig. 11(b) indicate that the $n = n^\star$ mode decays to zero, while the $n = 222$, 223, and 224 modes grow to large values. The dynamics are extremely noisy in this case, even after averaging over 180 runs, so that it is impossible to determine a single selected wave number from the structure function. In spite of this, it is clear that the suppression of modes near the critical one seen in the original dynamics (Fig. 6) is a direct consequence of the large nonlinear excitations at small n. If these excitations are removed, the most probable wave number is much closer to the critical wave number.

In the following subsections, we perform a detailed numerical analysis of the nonlinear terms in Eq. (18) for $n \leqslant n_E^-$ as well as modes close to the critical mode, for $\alpha = 0.20$ and $\varepsilon = 0.0001$. We use a small noise strength so that we are able to distinguish between the linear and nonlinear regimes. For this noise strength, the most probable wave number is $n_S(0.0001, T_S) = 215$. We will show that the critical mode initially drives the nonlinear growth of the small n modes. When the small n modes become large, they cause the decay of the modes near n_c. We will then consider the effect of the small n modes on the $n = n_S$ mode and show that the small n modes drive the *growth* of this mode (or the $n^\star$ mode when $\varepsilon \geqslant \varepsilon_{\min}$).

A. Nonlinear growth of long-wavelength modes and consequences for Eckhaus modes

We write Eq. (18) for small n, disregarding terms like $\langle \widetilde{u}_n \widetilde{\zeta}_{-n} \rangle$ and $\langle \widetilde{u}_{-n} \widetilde{\zeta}_n \rangle$. For concreteness, we focus on the case $n = 1$. The analysis is similar for all modes with $n \leqslant n_E^-$,

$$\dot{S}_1(t) = 2\sigma_1 S_1(t) + \sum_{n_1=1}^{N/2-1} (S_{1,n_1} + S_{-1,n_1}) = 2\sigma_1 S_1(t) + \mathcal{N}_1.$$

(19)

We know from Sec. III that the effect of the noise is significant only in the nonlinear regime. The nonlinear term in Eq. (19) is

$$
\begin{aligned}
\mathcal{N}_1 &= \sum_{n_1=1}^{N/2-1} (S_{1,n_1} + S_{-1,n_1}) \\
&= S_{1,1} + S_{-1,1} + S_{1,2} + S_{-1,2} + \cdots \\
&\quad + \underbrace{S_{1,n_E^-} + S_{-1,n_E^-} + \cdots + S_{1,n_E^+} + S_{-1,n_E^+}}_{\text{Eckhaus stable modes}} + \cdots .
\end{aligned}
$$

(20)

We expect that the largest terms in Eq. (20) are the ones with $n_E^- \leqslant n_1 \leqslant n_E^+$. These terms represent the interactions between the $n = 1$ mode and the Eckhaus stable modes. Out of these terms, the terms with n_1 close to n_c have the largest magnitude at the start of the nonlinear regime. From the definition of $S_{\pm n, n_1}$, we see that the $n = 1$ mode is coupled to the $n = n_c$ mode when $n_1 = n_c - 1$, n_c or $n_c + 1$. These terms evaluate to

$$S_{1,n_c} + S_{-1,n_c} + S_{1,n_c-1} + S_{-1,n_c+1}.$$

(21)

We further note that $S_{1,n_c} = S_{-1,n_c+1}$ and $S_{-1,n_c} = S_{1,n_c-1}$. Hence, the nonlinear terms coupling $n = 1$ with $n = n_c$ are

$$
\begin{aligned}
2(S_{1,n_c} + S_{-1,n_c}) &= 4(2\pi/L)^2 [n_c(n_c + 1)\mathrm{Re}\langle \widetilde{u}_{n_c} \widetilde{u}_{-n_c-1} \widetilde{u}_1 \rangle \\
&\quad + n_c(n_c - 1)\mathrm{Re}\langle \widetilde{u}_{n_c} \widetilde{u}_{-n_c+1} \widetilde{u}_{-1} \rangle],
\end{aligned}
$$

(22)

where we have used Eqs. (8) and (9) for the nth component of the DFT of the spatial derivative $\partial_x u$. These terms represent the net effect of the critical mode on the time evolution of S_1.

At the same time, the $n = 1$ mode contributes to the equation of motion of S_{n_c}, which is the component of the structure function corresponding to the critical mode. The equation of motion for S_{n_c} is

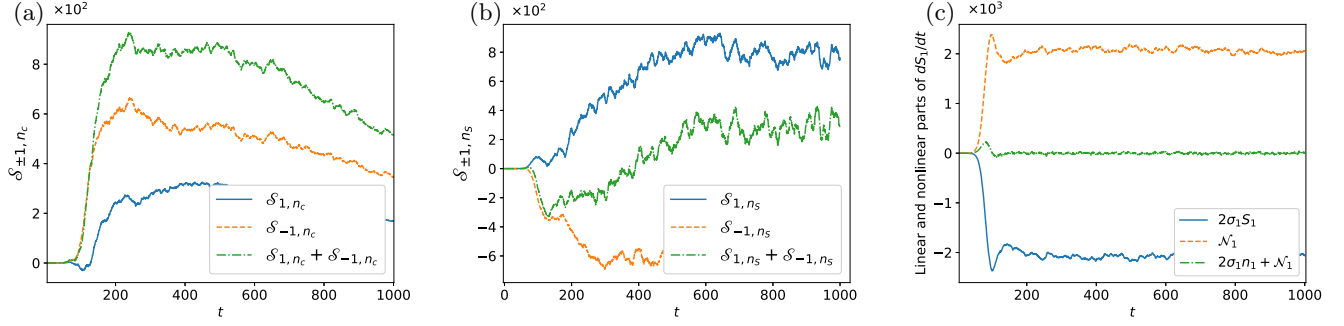$$\dot{S}_{n_c}(t) = 2\sigma_{n_c} S_{n_c}(t) + \mathcal{N}_{n_c}.$$

(23)

FIG. 12. (a) Terms in $\mathcal{N}_1$ that contain $\widetilde{u}_{n_c}$ and their sum. (b) Terms in $\mathcal{N}_1$ that contain $\widetilde{u}_{n_S}$ and their sum. (c) Linear and nonlinear parts of Eq. (19). The dash-dotted curve is their sum, i.e., the time derivative of S_1.

As before, we can write the nonlinear term $\mathcal{N}_{n_c}$ as

$$
\begin{aligned}
\mathcal{N}_{n_c} &= \sum_{n_1=1}^{N/2-1} (\mathcal{S}_{n_c,n_1} + \mathcal{S}_{-n_c,n_1}) \\
&= \underbrace{\mathcal{S}_{n_c,1} + \mathcal{S}_{-n_c,1} + \mathcal{S}_{n_c,2} + \mathcal{S}_{-n_c,2}}_{\text{long-wavelength modes}} + \cdots \\
&\quad + \mathcal{S}_{n_c,n_E^-} + \mathcal{S}_{-n_c,n_E^-} + \cdots + \mathcal{S}_{n_c,n_E^+} + \mathcal{S}_{-n_c,n_E^+} + \cdots .
\end{aligned}
\tag{24}
$$

The terms in Eq. (24) depending on $\widetilde{u}_1$ are

$$
\mathcal{S}_{n_c,1} + \mathcal{S}_{-n_c,1} + \mathcal{S}_{-n_c,n_c-1} + \mathcal{S}_{-n_c,n_c+1}.
\tag{25}
$$

Again, from the definition of $\mathcal{S}_{\pm n,n_1}$, it follows that $\mathcal{S}_{n_c,1} = \mathcal{S}_{-n_c,n_c+1}$ and $\mathcal{S}_{-n_c,1} = \mathcal{S}_{-n_c,n_c-1}$. The nonlinear terms of Eq. (25) then add up to

$$
\begin{aligned}
2(\mathcal{S}_{n_c,1} + \mathcal{S}_{-n_c,1}) &= 4(2\pi/L)^2 \\
&\times [(n_c + 1) \times \operatorname{Re}\langle \widetilde{u}_1 \widetilde{u}_{-n_c-1} \widetilde{u}_{n_c} \rangle \\
&- (n_c - 1) \times \operatorname{Re}\langle \widetilde{u}_{n_c-1} \widetilde{u}_1 \widetilde{u}_{-n_c} \rangle].
\end{aligned}
\tag{26}
$$

Comparing Eqs. (22) and (26), we see that $\mathcal{S}_{1,n_c}$ and $\mathcal{S}_{n_c,1}$ are both proportional to $\operatorname{Re}\langle \widetilde{u}_1 \widetilde{u}_{-n_c-1} \widetilde{u}_{n_c} \rangle$, and they have the same sign. Similarly, $\mathcal{S}_{-1,n_c}$ and $\mathcal{S}_{-n_c,1}$ are both proportional to $\operatorname{Re}\langle \widetilde{u}_{n_c} \widetilde{u}_{-n_c+1} \widetilde{u}_{-1} \rangle$, *but they have opposite signs*. We numerically evaluate each of these quantities for $\alpha = 0.20$ and $\varepsilon = 0.0001 < \varepsilon_{\min}$.

First, we plot $\mathcal{S}_{1,n_c}$ and $\mathcal{S}_{-1,n_c}$ as well as their sum as a function of time in Fig. 12(a). After about $t = 80$, both $\mathcal{S}_{1,n_c}$ and $\mathcal{S}_{-1,n_c}$ (and hence their sum) are positive. Thus, the net contribution of the critical mode to the equation of motion of S_1 is positive.

A short time later, Eckhaus modes further from n_c become important, and other terms in Eq. (20) become large. As an example, we show the effect of the $n = n_S$ mode on the time evolution of S_1 in Fig. 12(b). We see that $\mathcal{S}_{1,n_S}$ is positive, but $\mathcal{S}_{-1,n_S}$ is negative. However, their sum is almost always positive, although it is smaller than the corresponding contribution from the critical mode.

Having studied some of the typical terms arising in Eq. (20), we plot the full nonlinear term $\mathcal{N}_1$ and the linear term, i.e., $2\sigma_1 S_1$, in Fig. 12(c). In the same plot, we show the total time derivative of S_1, which is simply the sum $2\sigma_1 S_1 + \mathcal{N}_1$. The linear term $2\sigma_1 S_1$ is always negative because

the growth rate σ_1 is negative and S_1 is positive by definition. The total nonlinear term $\mathcal{N}_1$ is always positive. Most importantly, starting at $t \approx 80$, the magnitude of the nonlinear term becomes slightly greater than that of the linear one, and the sum of the two is positive (green dash-dotted line). Note that this is around the same time that the nonlinear terms in dS_1/dt arising from the critical mode become nonzero. This shows that the interaction between the $n = 1$ mode and the critical mode is responsible for the initial increase in S_1. Later, other Eckhaus modes become active and sustain the growth of S_1 until $t \approx 100$. Shortly after, the linear and nonlinear parts balance each other and S_1 reaches a steady nonzero value.

Let us now return to Eq. (26). We plot each of the terms $\mathcal{S}_{n_c,1}$ and $\mathcal{S}_{-n_c,1}$, along with their sum, in Fig. 13(a). We expect $\mathcal{S}_{n_c,1}$ to be positive and $\mathcal{S}_{-n_c,1}$ to be negative, as discussed above. This is indeed what we observe. The sum of the two is *negative*, and we conclude that the total contribution of the $n = 1$ mode to the time derivative of S_{n_c} is negative. Figures 12(a) and 13(a) and the discussion above have an important implication: *The nonlinear couplings between the $n = 1$ and $n = n_c$ modes assist the growth of S_1, but oppose the growth of S_{n_c}.*

The next piece of the puzzle is to understand why the $n = n_S$ mode persists, even though the critical mode and modes close to it decay. In analogy with Eq. (26), the net effect of the $n = 1$ mode on the evolution of the $n = n_S$ mode is

$$
\begin{aligned}
2(\mathcal{S}_{n_S,1} + \mathcal{S}_{-n_S,1}) &= 4\left(\frac{2\pi}{L}\right)^2 [(n_S + 1) \times \operatorname{Re}\langle \widetilde{u}_1 \widetilde{u}_{-n_S-1} \widetilde{u}_{n_S} \rangle \\
&- (n_S - 1) \times \operatorname{Re}\langle \widetilde{u}_1 \widetilde{u}_{n_S-1} \widetilde{u}_{-n_S} \rangle].
\end{aligned}
\tag{27}
$$

The time evolution of $\mathcal{S}_{n_S,1}$ and $\mathcal{S}_{-n_S,1}$ along with their sum is shown in Fig. 13(b). This time, $\mathcal{S}_{-n_S,1}$ becomes positive after $t \approx 230$, and the sum $\mathcal{S}_{n_S,1} + \mathcal{S}_{-n_S,1}$ is positive. Thus, the nonlinear interactions between $n = 1$ and $n = n_S$ contribute positive terms to the time derivative of S_{n_S} and hence assist the growth of the $n = n_S$ mode.

We now evaluate and plot the full right-hand side of Eq. (12) for different values of n in the Eckhaus band. In general, we see that the time derivative of the structure function becomes more and more negative as n is increased beyond n_c. We illustrate this for $n = 232$ (solid blue line) in Fig. 13(c). For $n = n_c$, the total time derivative $\frac{dS_{n_c}}{dt}$ dips slightly below zero around $t \approx 200$, and remains negative. Note that this occurs at about the same time that the contribution of the
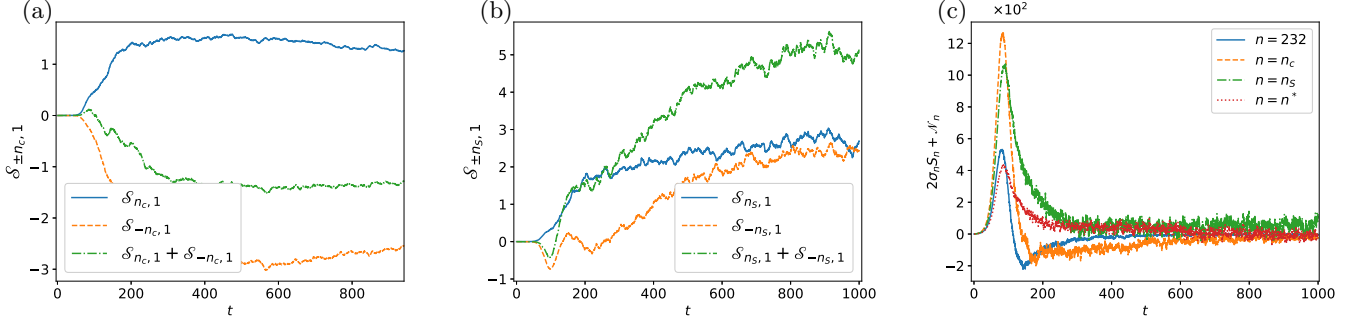
FIG. 13. (a) $\mathcal{S}_{n_c,1}$ and $\mathcal{S}_{-n_c,1}$ as a function of time. Their sum represents the total contribution of $\widetilde{u}_1$ to $\dot{S}_{n_c}$ and is negative after $t \approx 180$. (b) $\mathcal{S}_{n_S,1}$ and $\mathcal{S}_{-n_S,1}$ as a function of time. Their sum represents the total contribution of $\widetilde{u}_1$ to $\dot{S}_{n_S}$ and is always positive. (c) $\dot{S}_n = 2\sigma_n S_n + \mathcal{N}_n$ as a function of time for various values of n. It is negative for $n = n_c$ and $n = 232$ after a particular time, but positive for n_S and $n^\star$.

$n = 1$ mode to dS_{n_c}/dt becomes negative [see the green curve in Fig. 13(a)]. This suggests that the growth of the small n modes in the nonlinear regime is directly responsible for the damping of the critical mode.

On the other hand, the time derivative of S_{n_S} stays nonnegative throughout. We also show the time derivative of $S_{n^\star}$ (dash-dotted line). $dS_{n^\star}/dt$ is non-negative for almost all t, but its magnitude is less than that of dS_{n_S}/dt, which explains why $n_S = 215 \neq n^\star$ for $\varepsilon = 0.0001$.

B. Significance of noise strength and control parameter in exciting small wave-number modes

The extent to which the modes with $n < n_E^-$ are excited by the noise depends on ε. To understand this dependence, we again focus on S_1. We compute $S_1(t = T_S)$ for a wide range of ε and plot it in Fig. 14. The value of $S_1(t = T_S)$ increases as ε is increased. The increasing strength of the $n < n_E^-$ modes as ε increases drives $n_S(\varepsilon, T_S)$ closer and closer to $n^\star$, with n_S becoming *equal to* $n^\star$ when $\varepsilon \geqslant \varepsilon_{\min}$. It would be interesting to examine the dependence of all small n modes on the noise strength, as well as on the value of α. This is beyond the scope of the present paper and is saved for future work.

We can also provide a qualitative explanation for why the selected wave number decreases as we decrease α. We know that the width of the Eckhaus band increases as α decreases. Hence, the evolution equation for S_1 contains more terms that mix $\widetilde{u}_1$ with Eckhaus stable modes. Although we are unable to

give a rigorous mathematical proof, our simulations show that the larger number of mixing terms causes a larger excitation of the $(n < n_E^-)$ modes.

We repeat the simulations of Sec. IV A for $\alpha = 0.17$ and the same noise strength ($\varepsilon = 0.0001$). We show the linear and nonlinear terms in $\dot{S}_1$, as well as their sum in Fig. 15. The linear term is negative while the nonlinear term is positive, as in Fig. 12(a). The sum of the linear and nonlinear terms is positive at short times. *Comparing the scale of the vertical axis in Fig. 12(c) with that of Fig. 15 shows that $\dot{S}_1$ (and hence S_1) is larger for $\alpha = 0.17$ than for $\alpha = 0.20$, for the same noise strength.* This in turn, ensures that modes near the critical mode are damped to a larger extent as α is decreased below α_c. As a result, n_S decreases below n_c as α is decreased below α_c for fixed noise strength.

V. CONCLUSIONS

In this work, we have identified the mechanism of noise-induced wave-number selection in a simple model of pattern formation. We have shown that the noise inhibits the nonlinear growth of modes near the critical mode, and enhances the growth of modes smaller than the critical wave number. The amplification of very long-wavelength perturbations is responsible for the above effects. We have shown that if long-wavelength excitations are suppressed, the selected wave numbers are close to the critical wave number. Together,
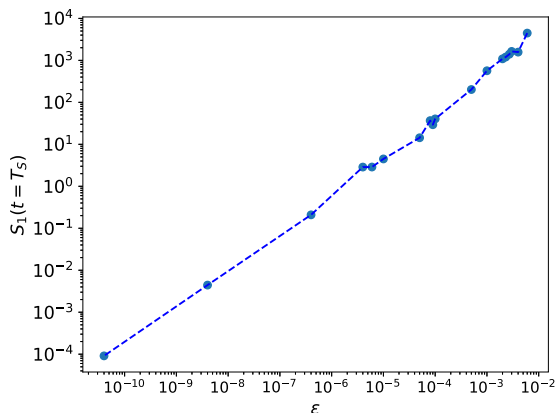

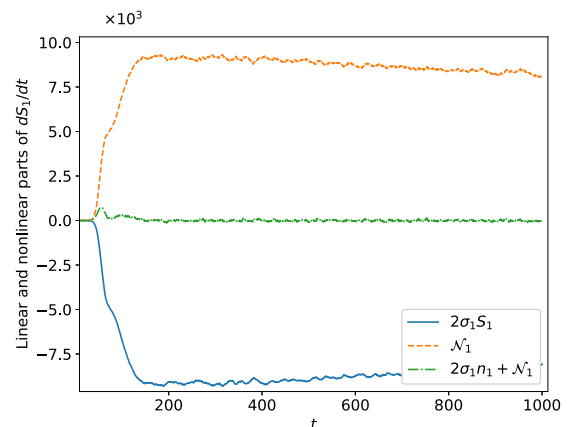FIG. 14. $S_1(t = T_S)$ for different noise strengths, and $\alpha = 0.20$.

FIG. 15. Linear and nonlinear terms in $\frac{d}{dt}S_1$ and their sum for $\alpha = 0.17$ and $\varepsilon = 0.0001$.

these findings indicate that the coupling between modes with small wave numbers and the Eckhaus stable modes is the most important factor in determining the selected state.

It is important to address some shortcomings of our numerics. First, we are unable to draw definitive conclusions about selection in the weak noise regime for reasons explained in Sec. III C. This is purely due to finite computational resources. If we somehow increase T, it is possible that a stationary histogram peaked at $n^\star$ could be attained for very small values of ε. Alternatively, it is possible that the dominant wave number determined from the structure function, i.e., n_S, approaches $n^\star$ for small ε as $T_S \to \infty$. With our current resources and algorithms, it is not possible to confirm these hypotheses numerically, and we have to restrict our attention exclusively to the strong noise regime.

Secondly, the evolution of the structure function is very noisy, in spite of averaging over 180 independent trajectories. On the other hand, the histograms of Ref. [15] are quite smooth. This is because the histograms were obtained by determining the state of the system at each time step over one trajectory of length $\sim 10^8 \Delta t$, which is equivalent to taking 10^8 independent measurements of the state of the system. In contrast, for the structure function approach, one needs to find the *ensemble* average of the quantity $|\widetilde{u}_n(t)|^2$, which fluctuates rapidly from one time step to the next. In addition, computational restrictions prevent us from running more than 180 independent trajectories. Thus, the temporal averaging over a long run leads to very smooth statistics, while averaging over trajectories does not. However, in spite of the noisiness, one can obtain new insights into the mechanism of wave-number selection from the structure function dynamics that cannot be gained solely from the stationary histograms of our previous work.

Finally, it is worth mentioning that the large noise-induced nonlinear excitations at small wave numbers seen here may be related to the existence of chaotic solutions as $\alpha \to 0$. These chaotic solutions are a distinctive feature of the SKS equation, and more studies of the stochastic SKS equation are needed in the $\alpha < 0.16$ regime. It would be interesting to investigate noise-driven selection in other nonpotential models that do not possess chaotic solutions.

Another promising direction is to explore stochastic dynamics in higher dimensions and in the more realistic situations described in the Introduction. We also anticipate that the large noise strengths used here, which may be unphysical for some systems, will be relevant to biological processes, where the noise is known to be large [24].

APPENDIX A: SOLVING PARTIAL DIFFERENTIAL EQUATIONS IN FOURIER SPACE

We derive the appropriate discrete Fourier transforms of the various derivatives of the field $u(x, t)$ needed for the SKS problem. We closely follow the treatment given in Ref. [21] of the manuscript. The field $u(x, t)$ is defined for $0 \leqslant x \leqslant L$ with periodic boundary conditions $u(x + L, t) = u(x, t)$ so that

$$u(x, t) = \sum_{n=-\infty}^{\infty} \widetilde{u}_n(t) e^{\frac{2\pi i n x}{L}} \tag{A1}$$

with the Fourier coefficients given by

$$\widetilde{u}_n(t) = \frac{1}{L} \int_0^L e^{-\frac{2\pi i n x}{L}} u(x, t) dx. \tag{A2}$$

Now, we approximate $u(x, t)$ by N discrete samples $u_m(t) = u(mL/N, t)$ for $m = 0, 1, \ldots, N - 1$, and the $\widetilde{u}_n(t)$ are approximated using the discrete Fourier transform (DFT), defined as

$$\widetilde{u}_n(t) = \sum_{m=0}^{N-1} u_m(t) e^{-\frac{2\pi i n m}{N}}. \tag{A3}$$

The values of $u_m(t)$ can be obtained from the inverse discrete Fourier transform (IDFT),

$$u_m(t) = \frac{1}{N} \sum_{n=0}^{N-1} \widetilde{u}_n(t) e^{\frac{2\pi i n m}{N}}. \tag{A4}$$

(The placement of the prefactor $1/N$ is a matter of convention, and we have chosen the convention consistent with NumPy's implementation of the DFT.) The $\widetilde{u}_n$'s can be obtained from the u_m's and vice versa in $O(N \ln N)$ operations using the fast Fourier transform (FFT). In what follows, we will not explicitly indicate the dependence on t for convenience. It
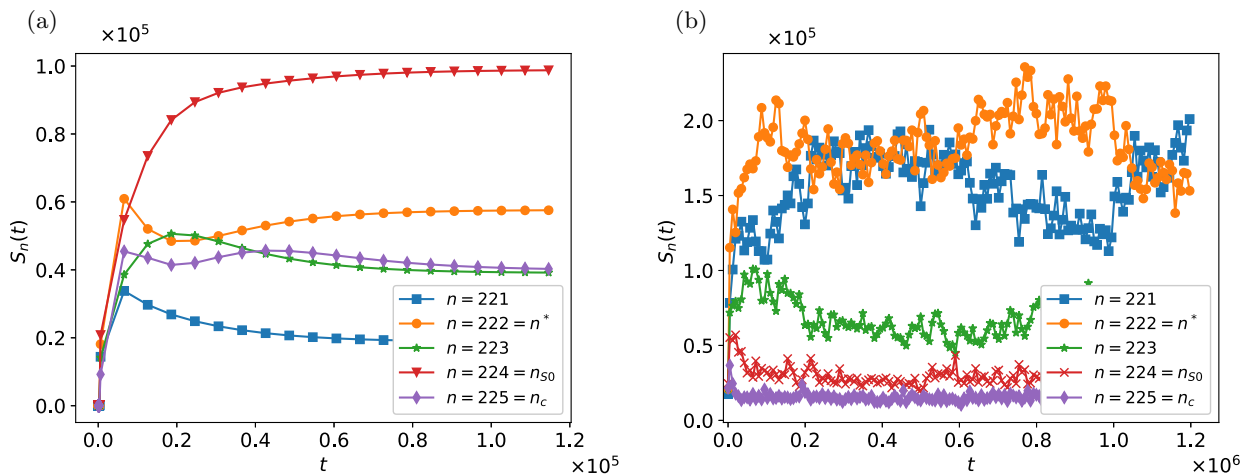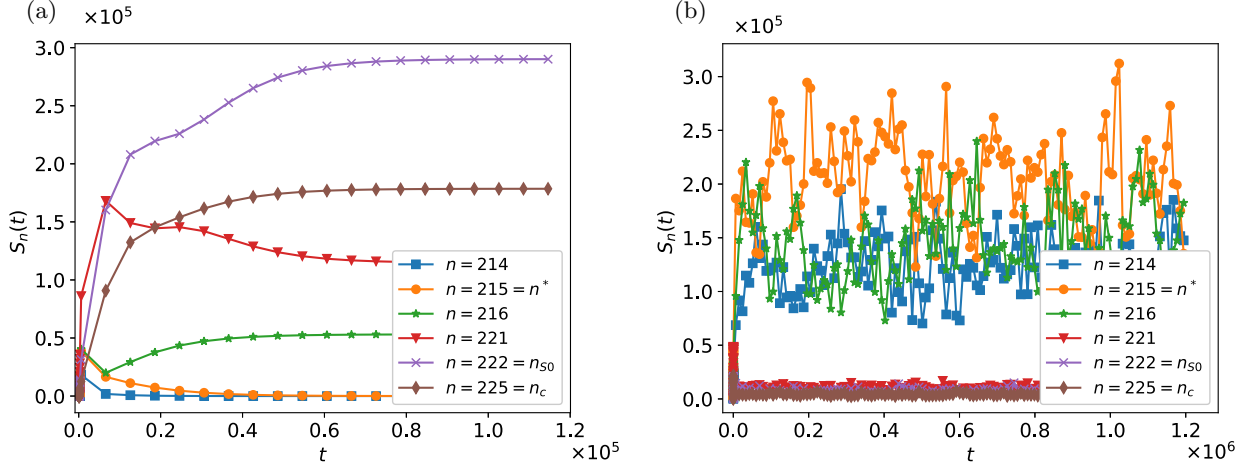

FIG. 16. S_n as a function of time for $\alpha = 0.24$. (a) $\varepsilon = 0.0$. (b) $\varepsilon = 0.0005$.

FIG. 17. S_n as a function of time for $\alpha = 0.22$. (a) $\varepsilon = 0.0$. (b) $\varepsilon = 0.0025$.

should be understood that the u_m's and $\widetilde{u}_n$'s are functions of time.

To compute derivatives such as $u'(x)$, we need more than just the discrete samples u_m. We need to obtain a continuous interpolation *between* sample points and *differentiate this interpolation*. We use a technique called trigonometric interpolation. First, we note that replacing n in Eq. (A14) by $n + lN$, where l is an integer, leaves the sample values u_m unchanged. However, it changes the values of the derivatives of u between the sample points, because it causes $u(x)$ to oscillate between sample points. This is called *aliasing*. To resolve this ambiguity, we assume a more general interpolation obtained by substituting $m = Nx/L$ into Eq. (A14) and allowing an arbitrary aliasing integer l_n for each $\widetilde{u}_n$,

$$u(x) = \frac{1}{N} \sum_{n=0}^{N-1} \widetilde{u}_n e^{\frac{2\pi i}{L}(n+l_n N)x}, \qquad (A5)$$

where the l_n's are integers. We now impose the condition that the interpolating function undergoes "minimal oscillation" between sample points. This is equivalent to minimizing the

spatial average of the squared slope $\frac{1}{L} \int_0^L |u'(x)|^2 dx$. Substituting Eq. (A5) into this expression and simplifying gives

$$\frac{1}{L} \int_0^L |u'(x)|^2 dx = \left(\frac{2\pi}{LN}\right)^2 \sum_{n=0}^{N-1} |\widetilde{u}_n|^2 (n + l_n N)^2. \qquad (A6)$$

We see that the average squared slope is minimized by those l_n's that minimize $(n + l_n N)^2$ for each n. For $0 \leqslant n < N/2$, this quantity is minimum for all $l_n = 0$. For $N/2 < n < N$, the quantity is minimized by setting all the l_n's to -1. The situation is more complicated when N is even and $n = N/2$ because now the quantity $(n + l_n N)^2$ can be minimized by either $l_{N/2} = 0$ or -1. To overcome this issue, we split the $n = N/2$ term between the cases $l_n = 0$ and -1 in the form $\widetilde{u}_{N/2}[v e^{i\pi Nx/L} + (1 - v)e^{-i\pi Nx/L}]$. The contribution of this term to the mean-squared slope is

$$\frac{1}{N^2}\left(\frac{\pi N}{L}\right)^2 |\widetilde{u}_{N/2}|^2 [v^2 + (1 - v)^2], \qquad (A7)$$
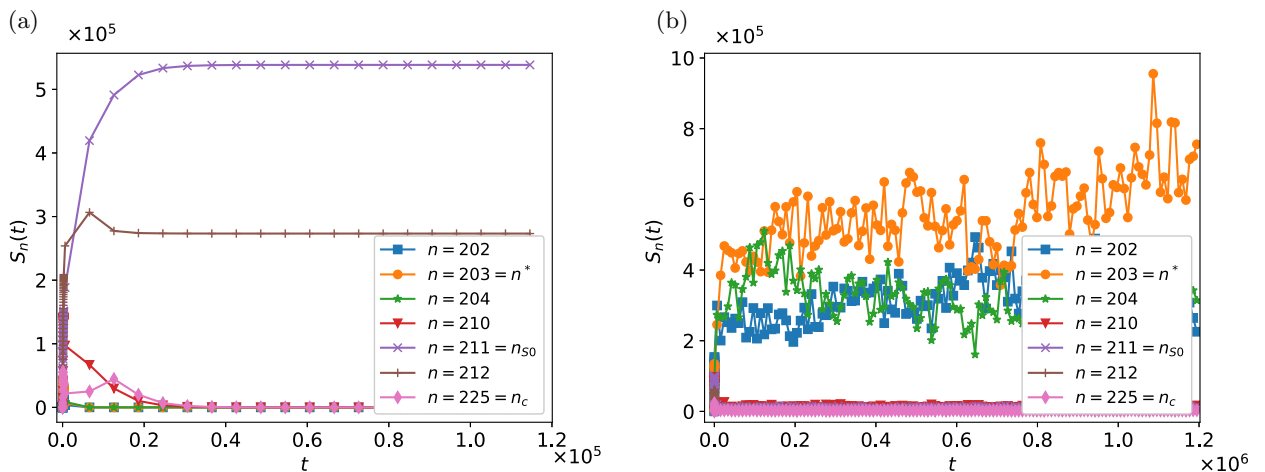
FIG. 18. S_n as a function of time for $\alpha = 0.17$. (a) $\varepsilon = 0.0$. (b) $\varepsilon = 0.005$.
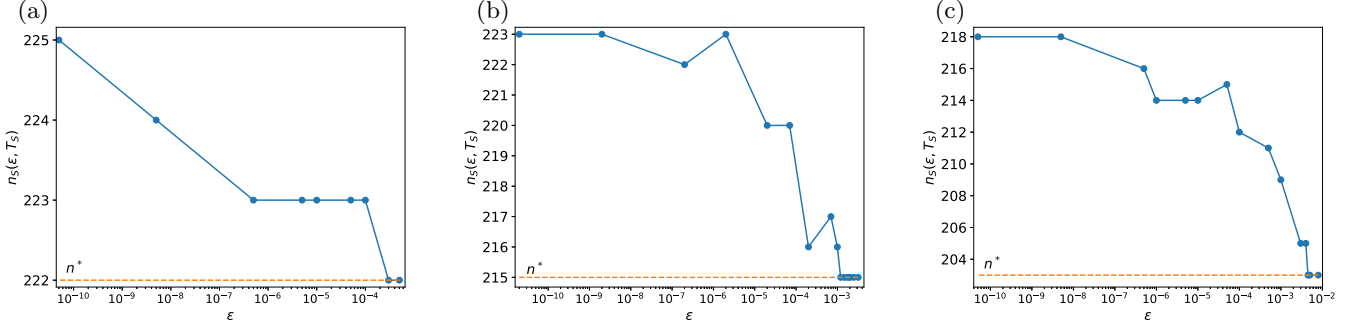
FIG. 19. $n_S(\varepsilon, T_S)$ for (a) $\alpha = 0.24$. (b) $\alpha = 0.22$. (c) $\alpha = 0.17$.

which is minimized by $v = 1/2$. The minimum oscillation interpolation of $u(x)$ is then

$$Nu(x) = \widetilde{u}_0 + \sum_{0<n<N/2} \widetilde{u}_n e^{2\pi i n x/L}$$
$$+ \sum_{N/2+1<n<N} \widetilde{u}_n e^{2\pi i(n-N)x/L} + \widetilde{u}_{N/2}$$
$$\times \cos(\pi N x/L). \tag{A8}$$

From this expression, the spatial derivatives can be calculated easily. For example, differentiating Eq. (A8) gives

$$Nu'(x) = \sum_{0<n<N/2} \frac{2\pi i n}{L} \widetilde{u}_n e^{+\frac{2\pi i n x}{L}}$$
$$+ \sum_{N/2+1<n<N} \frac{2\pi i(n-N)}{L} \widetilde{u}_n e^{\frac{2\pi i(n-N)x}{L}}$$
$$- \frac{\pi N}{L} \widetilde{u}_{N/2} \sin\left(\frac{\pi N x}{L}\right). \tag{A9}$$

Evaluating at the sample points $x = mL/N$, we get

$$Nu'_m = \sum_{0<n<N/2} \frac{2\pi i n}{L} \widetilde{u}_n e^{+\frac{2\pi i n m}{N}}$$
$$+ \sum_{N/2+1<n<N} \frac{2\pi i(n-N)}{L} \widetilde{u}_n e^{\frac{2\pi i(n-N)m}{N}} \tag{A10}$$

since the derivative of the $N/2$ term vanishes at the sample points. Noting that $e^{\frac{2\pi i(n-N)m}{N}} = e^{\frac{2\pi n m}{N}}$, we get

$$Nu'_m = \sum_{0<n<N/2} \frac{2\pi i n}{L} \widetilde{u}_n e^{+\frac{2\pi i n m}{N}}$$
$$+ \sum_{N/2+1<n<N} \frac{2\pi i(n-N)}{L} \widetilde{u}_n e^{\frac{2\pi i n m}{N}}. \tag{A11}$$

We set $u'_m = v_m$ and let the DFT of u'_m be denoted by $\widetilde{v}_n$. Then, comparing with the definition of the IDFT, Eq. (A14), it is seen that
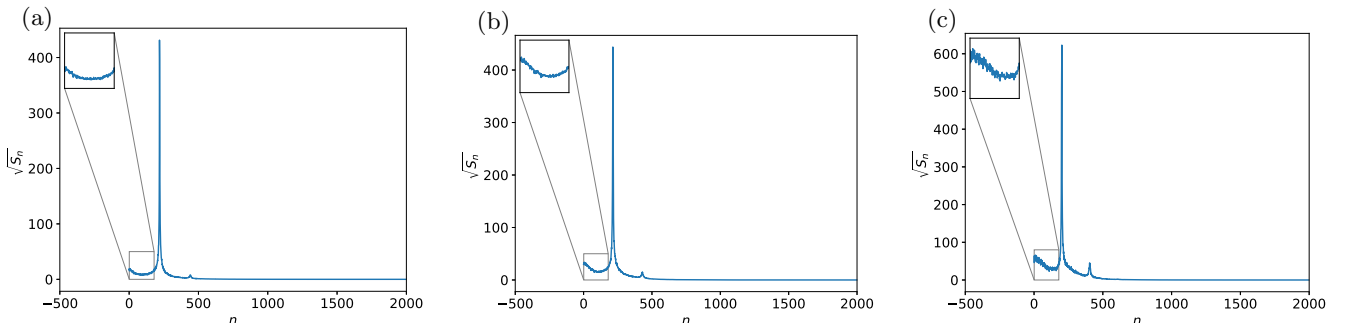
$$\widetilde{v}_n = \frac{2\pi i n}{L} \widetilde{u}_n \quad \text{if } 0 < n < N/2$$
$$= \frac{2\pi i(n-N)}{L} \widetilde{u}_n \quad \text{if } N/2 + 1 < n < N \tag{A12}$$
$$= 0 \text{ if } n = 0 \text{ or } n = N/2.$$

This can be written compactly as

$$\widetilde{v}_n = \frac{2\pi i n}{L} \widetilde{u}_n; \quad n = 1, \ldots, N/2 - 1, -N/2 + 1, \ldots, -1 \tag{A13}$$

with $\widetilde{v}_0$ and $\widetilde{v}_{N/2}$ equal to zero as before. To maintain consistency, it is also customary to write Eq. (A14) as

$$u_m(t) = \frac{1}{N} \sum_{n=-N/2}^{N/2-1} \widetilde{u}_n(t) e^{\frac{2\pi i n m}{N}}. \tag{A14}$$

FIG. 20. $\sqrt{S_n}$ as a function of n for (a) $\alpha = 0.24$, $\varepsilon = 0.0005$. (b) $\alpha = 0.22$, $\varepsilon = 0.0025$. (c) $\alpha = 0.17$, $\varepsilon = 0.005$. Inset: excitation of small wave-number modes.
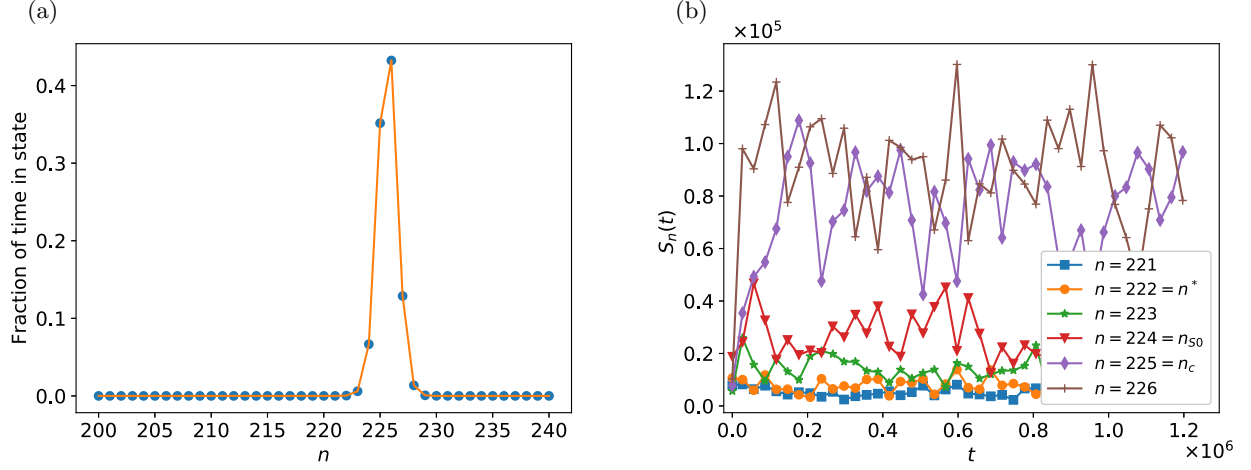
(a)

(b)

FIG. 21. (a) Long-time probability distribution of final states for $\alpha = 0.24$, $\varepsilon = 0.0005$ with the first 50 modes suppressed. (b) S_n as a function of time.

Similarly, the second and fourth spatial derivatives are

$$u_m'' = -\sum_{n=-N/2}^{N/2-1} \left(\frac{2\pi n}{L}\right)^2 \widetilde{u}_n e^{\frac{2\pi imn}{N}} \tag{A15}$$

and

$$u_m'''' = \sum_{n=-N/2}^{N/2-1} \left(\frac{2\pi n}{L}\right)^4 \widetilde{u}_n e^{\frac{2\pi imn}{N}}. \tag{A16}$$

We can now derive the DFT of the nonlinear term in the SKS equation, i.e., $(\partial_x u)^2 = v_m^2$. From Eq. (7), we have

$$\widetilde{\mathbf{N}}_n = \sum_{m=0}^{N-1} (\partial_x u)_m^2 e^{-2\pi imn/N}$$
$$= \sum_{m=0}^{N-1} v_m^2 e^{-2\pi imn/N}. \tag{A17}$$

Using the fact that $v_m = \frac{1}{N} \sum_{n=-N/2}^{N/2-1} \widetilde{v}_n e^{\frac{2\pi inm}{N}}$, we get

$$\widetilde{\mathbf{N}}_n = \frac{1}{N^2} \sum_{m=0}^{N-1} \exp\left[-2\pi inm/N\right]$$
$$\times \sum_{n_1=-N/2}^{N/2-1} \widetilde{v}_{n_1} \exp\left[2\pi in_1m/N\right]$$
$$\times \sum_{n_2=-N/2}^{N/2-1} \widetilde{v}_{n_2} \exp\left[2\pi in_2m/N\right]. \tag{A18}$$

Performing the sum over m yields $N\delta_{n_1+n_2-n}$. The end result is

$$\widetilde{\mathbf{N}}_n = \frac{1}{N} \sum_{n_1=-N/2}^{N/2-1} \widetilde{v}_{n_1} \widetilde{v}_{n-n_1}. \tag{A19}$$
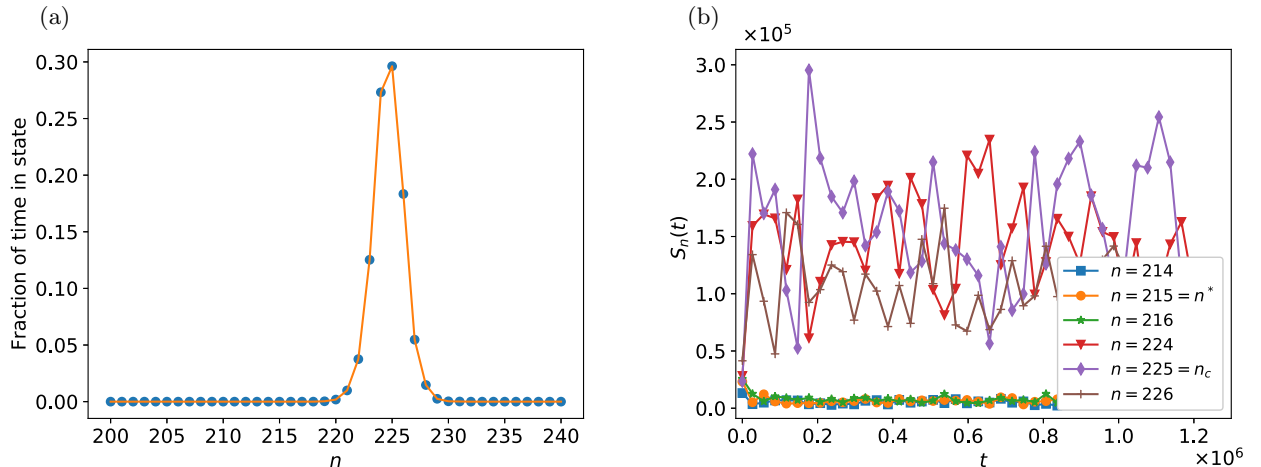
(a)

(b)

FIG. 22. (a) Long-time probability distribution of final states for $\alpha = 0.22$, $\varepsilon = 0.0025$ with the first 50 modes suppressed. (b) S_n as a function of time.
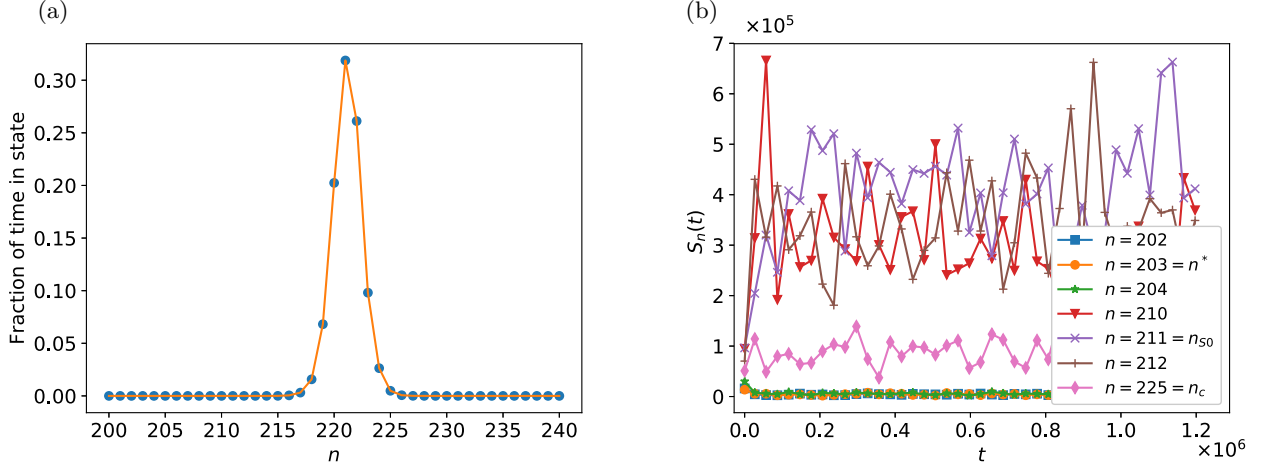
(a)

(b)

FIG. 23. (a) Long-time probability distribution of final states for $\alpha = 0.17$, $\varepsilon = 0.005$ with the first 50 modes suppressed. (b) S_n as a function of time.

APPENDIX B: DETERMINING THE APPROPRIATE RANGE OF α

As mentioned in the main manuscript, a variety of complicated configurations become possible when the second harmonic becomes linearly unstable along with the fundamental harmonic [18]. To determine the value of α when this occurs, we set the growth rates for a perturbation with wave number q and a perturbation with wave number $2q$ to zero for $\alpha = \alpha_2$,

$$\sigma(q) = -\alpha_2 + q^2 - q^4 = 0 \qquad \text{(B1)}$$

and

$$\sigma(2q) = -\alpha_2 + 4q^2 - 16q^4 = 0. \qquad \text{(B2)}$$

Solving these equations simultaneously gives $\alpha_2 = 4/25 = 0.16$ and $q = 1/\sqrt{5}$. Accordingly, we restrict our study to $0.16 < \alpha < 0.25$.

APPENDIX C: SIMULATIONS FOR OTHER VALUES OF α

Here we show our results for other values of the control parameter α. ε is greater than $\varepsilon_{\min}$ in all cases and hence $n_S = n^\star$. In Figs. 16, 17, and 18, we show the time evolution of $S_n(t)$ with and without noise for $\alpha = 0.24$, 0.22, and 0.17. For $\alpha = 0.24$ (Fig. 16), $n_{S0} = 224$ and $n^\star = 222$. For $\alpha = 0.22$ (Fig. 17), $n_{S0} = 222$ and $n^\star = 215$. Similar results are seen for $\alpha = 0.17$ (Fig. 18).

In Fig. 19, we show $n_S(\varepsilon, T_S)$ as a function of ε for $\alpha = 0.24$, 0.22, and 0.17.

Next we show the square root of the stationary structure function S_n versus n for the above values of α (Fig. 20). As shown in the main manuscript, there is a large amplification of modes near $n \approx 0$. The amplification is larger for smaller values of α.

Finally, we show how the stationary histograms and time evolution plots are modified when the modes between $n = 1$ and 50 are suppressed; see Figs. 21, 22, and 23.

APPENDIX D: MORE RESULTS FROM SEC. IV

The nonlinear growth of other small wave-number modes can be explained using a similar argument. For example, we also computed the time derivatives of S_{25} and S_{50}. These are also positive initially, and approach zero at late times, leading to a nonzero value of S_{25} and S_{50}, as seen in Fig. 24.

Finally, we give a heuristic explanation for why S_n decreases as n approaches n_E^- from the left. According to the discussion above, initially, the most important nonlinear terms in the equation for $\dot{S}_{25}$ are the ones involving $\widetilde{u}_{\pm n_c}$. These terms are proportional to $\mathrm{Re}\langle \widetilde{u}_{25} \widetilde{u}_{n_c} \widetilde{u}_{-250} \rangle$ and $\mathrm{Re}\langle \widetilde{u}_{-25} \widetilde{u}_{-200} \widetilde{u}_{n_c} \rangle$. In contrast, the corresponding terms in the equation for $\dot{S}_1$ are proportional to $\mathrm{Re}\langle \widetilde{u}_1 \widetilde{u}_{224} \widetilde{u}_{-n_c} \rangle$ and $\mathrm{Re}\langle \widetilde{u}_{-1} \widetilde{u}_{226} \widetilde{u}_{n_c} \rangle$. On average, $|\widetilde{u}_{224}|$ and $|\widetilde{u}_{226}|$ are likely to be larger than $|\widetilde{u}_{200}|$ and $|\widetilde{u}_{250}|$ (at the end of the linear regime). This means that the nonlinear terms in $\dot{S}_1$ for a fixed n_1 are generally larger than the corresponding terms in $\dot{S}_{25}$ and $\dot{S}_{50}$. The overall result is that $\dot{S}_{25}$ and $\dot{S}_{50}$ are always smaller than $\dot{S}_1$. In general, we observe that $|\dot{S}_n|$ decreases as n approaches the Eckhaus band from the left. For this reason, S_n in Fig. 10 decreases with n for $n < n_E^-$.
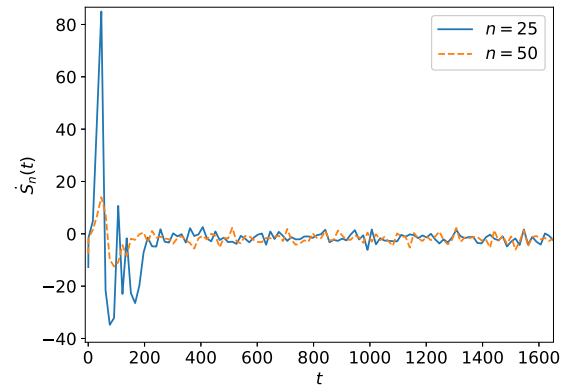

FIG. 24. dS_n/dt with $n = 25$ and 50 for $\alpha = 0.20$ and $\varepsilon = 0.0001$.

[1] M. C. Cross and H. Greenside, *Pattern Formation and Dynamics in Nonequilibrium Systems* (Cambridge University Press, New York, 2009).

[2] V. Eckhaus, *Studies in Nonlinear Stability Theory* (Springer-Verlag, Berlin, 1965).

[3] K. A. Jackson and J. D. Hunt, Trans. Metall. Soc. AIME **236**, 1129 (1966).

[4] J. M. Flesselles, A. J. Simon, and A. J. Libchaber, Adv. Phys. **40**, 1 (1991).

[5] A. J. Simon, J. Bechhoefer, and A. J. Libchaber, Phys. Rev. Lett. **61**, 2574 (1988).

[6] D. S. Cannell, M. A. Dominguez-Lerma, and G. Ahlers, Phys. Rev. Lett. **50**, 1365 (1983).

[7] L. Kramer, E. Ben-Jacob, H. Brand, and M. C. Cross, Phys. Rev. Lett. **49**, 1891 (1982).

[8] P. C. Hohenberg, L. Kramer, and H. Riecke, Physica D **15**, 402 (1985).

[9] H. R. Schober, E. Allroth, K. Schroeder, and H. Müller-Krumbhaar, Phys. Rev. A **33**, 567 (1986).

[10] J. Swift and P. C. Hohenberg, Phys. Rev. A **15**, 319 (1977).

[11] M. Kerszberg, Phys. Rev. B **27**, 3909 (1983).

[12] M. Kerszberg, Phys. Rev. B **28**, 247 (1983).

[13] L. Qiao, Z. Zheng, and M. C. Cross, Phys. Rev. E **93**, 042204 (2016).

[14] D. Obeid, J. M. Kosterlitz, and B. Sandstede, Phys. Rev. E **81**, 066205 (2010).

[15] S. Saxena and J. M. Kosterlitz, Phys. Rev. E **100**, 022223 (2019).

[16] Y. Pomeau and P. Manneville, J. Phys. (Paris) **40**, 609 (1979).

[17] J. Viñals, E. Hernández-García, M. San Miguel, and R. Toral, Phys. Rev. A **44**, 1123 (1991).

[18] C. Misbah and A. Valance, Phys. Rev. E **49**, 166 (1994).

[19] I. Bena, C. Misbah, and A. Valance, Phys. Rev. B **47**, 7408 (1993).

[20] L. N. Trefethen, *Spectral Methods in MATLAB* (SIAM, Philadelphia, 2000).

[21] J. Shen, T. Tang, and L.-L. Wang, *Spectral Methods: Algorithms, Analysis and Applications* (Springer-Verlag, Berlin, 2011).

[22] L. Q. Chen and J. Shen, Comput. Phys. Commun. **108**, 147 (1998).

[23] J. Garcia-Ojalvo and J. M. Sancho, *Noise in Spatially Extended Systems* (Springer-Verlag, New York, 1999).

[24] L. S. Tsimring, Rep. Prog. Phys. **77**, 026601 (2014).